**ANKARA YILDIRIM BEYAZIT UNIVERSITY**

**GRADUATE SCHOOL OF NATURAL AND APPLIED SCIENCES**




# X-RAY RADIATION EFFECTS ON THE $CuInGaTe_2$ SEMICONDUCTOR DIODE PARAMETERS

**M.Sc. Thesis by**

**Semra ARSLAN**

**Department of Material Engineering**

**June, 2018**

**ANKARA**

# X-RAY RADIATION EFFECTS ON THE $CuInGaTe_2$ SEMICONDUCTOR DIODE PARAMETERS

**A Thesis Submitted to**

**The Graduate School of Natural and Applied Sciences of**

**Ankara Yıldırım Beyazıt University**

**In Partial Fulfillment of the Requirements for the Degree of Master of Science in Material Engineering, Department of Material Engineering**

**by**

**Semra ARSLAN**

**June, 2018**

**ANKARA**

## M.Sc. THESIS EXAMINATION RESULT FORM

We have read the thesis entitled **"X-RAY RADIATION EFFECTS ON THE $CuInGaTe_2$ SEMICONDUCTOR DIODE PARAMETERS"** completed by **SEMRA ARSLAN** under the supervision of **PROF. DR. GÜVEN ÇANKAYA** and we certify that in our opinion it is fully adequate, in scope and in quality, as a thesis for the degree of Master of Science.

Prof. Dr. Güven ÇANKAYA

Supervisor

Prof. Dr. Aytunç ATEŞ

Jury Member

Dr. Faculty Member Hanifi ÇİNİCİ

Jury Member

Prof. Dr. Fatih V. ÇELEBİ

Director

Graduate School of Natural and Applied Sciences

# ETHICAL DECLARATION

I hereby declare that, in this thesis which has been prepared in accordance with the Thesis Writing Manual of Graduate School of Natural and Applied Sciences,

- All data, information and documents are obtained in the framework of academic and ethical rules,
- All information, documents and assessments are presented in accordance with scientific ethics and morals,
- All the materials that have been utilized are fully cited and referenced,
- No change has been made on the utilized materials,
- All the works presented are original,

and in any contrary case of above statements, I accept to renounce all my legal rights.

# ACKNOWLEDGMENTS

Firstly, I would like to thank my supervisor, Prof. Dr. Güven ÇANKAYA for helps, guidance and support provided to me during my study. His guidance assisted me all the time of my research and while writing this thesis.

I would like to thank Dr. Faculty Member Süheyla AYTAÇ ARSLAN and her staff, who are the faculty members of the Ankara Yıldırım Beyazıt University Medical School, who helped me to do this work with the opportunities I have provided.

I would like to thank Dr. Betül KÜÇÜKÖZ for her contribution and great effort while preparing diode samples for my thesis. She supported me in my experimental study with a nice working atmosphere at Optical Materials Research Group (OMAG) of Physics Engineering Department, Ankara University.

Finally, I would like to thank my parents for understanding and support.

**2018, June** **Semra ARSLAN**

"This work was supported by Ankara Yıldırım Beyazıt University Projects Office. Project Number: 3371"

# X-RAY RADIATION EFFECTS ON THE $CuInGaTe_2$ SEMICONDUCTOR DIODE PARAMETERS


## ABSTRACT

In this study, the effect of ionizing X-Ray radiation on the electrical parameters of $CuInGaTe_2$ semiconductor diode was investigated. I-V measurements were taken for five different radiation values (200, 400, 600, 800 and 1000 centiGray (cGy)) in the laboratory environment. The diodes were irradiated with a 6 MV X-Ray generating linear accelerator (LINAC) and standard applicators of 10x10 $cm^2$ area size were used to shape the X-Ray during all irradiation. Electrical parameters such as the ideality factor, barrier height, and series resistance were obtained with the help of the forward bias I-V measurements before and after irradiation. Then these parameters were calculated by Cheung-Cheung method and it was observed that the results were compatible with each other. In addition, the interface states density was determined from the forward bias I-V characteristics. As the irradiation dose increased, the ideality factor increased and the barrier height decreased. This is due to the defects in the interface of the diodes and the increase in the intensity of the interface states. As the radiation dose increased, all series resistance values increased. This was attributed to a decrease in mobility and free carrier concentration. It was observed that the diode diverged from the ideal because of the defects that occurred after X-Ray irradiation. The results show that X-Ray radiation is effective on the electrical properties of diode. This feature demonstrates that the $CuInGaTe_2$ semiconductor diode can be used in X-Ray radiation detection devices.



**Keywords:** X-Ray radiation, Semiconductor diode, Barrier height, Ideality factor

# $CuInGaTe_2$ YARIİLETKEN DİYOT PARAMETRELERİNE X-IŞINI RADYASYONUNUN ETKİSİ

## ÖZ

Bu çalışmada $CuInGaTe_2$ yarıiletken diyotun elektriksel parametreleri üzerine iyonlaştırıcı X-Işını radyasyonunun etkisi araştırıldı. I-V ölçümleri laboratuvar ortamında beş farklı radyasyon değeri (200, 400, 600, 800 ve 1000 santiGray (cGy)) için alındı. Diyotlar, 6 MV X-Işını oluşturan bir lineer hızlandırıcı (LINAC) ile ışınlandı ve tüm ışınlamalar süresince X-Işınını şekillendiren 10x10 $cm^2$ alan boyutlarında standart aplikatörler kullanıldı. İdealite faktörü, bariyer yüksekliği, seri direnç gibi elektriksel parametreler ışınım öncesi ve sonrasında ileri beslem I-V ölçümleri yardımıyla elde edildi. Ardından Cheung-Cheung metoduyla bu parametreler hesaplandı ve sonuçların birbiriyle uyumlu olduğu gözlemlendi. Buna ilave olarak, arayüzey durumlarının yoğunluğu, düz beslem I-V karakteristiklerinden belirlendi. Işınlanma dozunun artışıyla idealite faktörünün arttığı, engel yüksekliğinin ise azaldığı gözlendi. Bu, diyotların arayüzeyinde oluşan kusurlara ve arayüz durumlarının yoğunluğundaki artışa bağlandı. Radyasyon dozunun artmasıyla, tüm seri direnç değerlerinde artış gözlendi. Bu durum, mobilite ve serbest taşıyıcı konsantrasyonunun azalmasına atfedildi. İyonlaştırıcı X-Işını ışınlamasından sonra oluşan kusurlardan dolayı diyotun ideallikten saptığı gözlendi. Sonuçlar, diyotun elektriksel özelliklerinin üzerinde X-Işını radyasyonunun etkili olduğunu göstermiştir. Bu özellik, $CuInGaTe_2$ yarıiletken diyotunun X-Işını radyasyon algılama aygıtlarında kullanılabileceğini ortaya koymaktadır.

**Anahtar Kelimeler:** X-Işını radyasyonu, Yarıiletken diyot, Bariyer yüksekliği, İdealite faktörü

# CONTENTS

M.Sc. THESIS EXAMINATION RESULT FORM ..... ii

ETHICAL DECLARATION ..... iii

ACKNOWLEDGMENTS ..... iv

ABSTRACT ..... v

ÖZ ..... vi

CONTENTS ..... vii

NOMENCLATURE ..... x

LIST OF TABLES ..... xiii

LIST OF FIGURES ..... xiv

**CHAPTER 1 - INTRODUCTION ..... 1**

1.1 A General View of Semiconductor Materials ..... 4

1.2 Review of Related Works ..... 5

1.3 Aim of the Study ..... 7

**CHAPTER 2 - SEMICONDUCTORS ..... 9**

2.1 Introduction ..... 9

2.1.1 Element Semiconductors ..... 9

2.1.2 Compound Semiconductors ..... 10

2.2 Energy Bands ..... 11

2.3 Insulator, Semiconductor, Conductor ..... 12

2.3.1 Intrinsic Semiconductors ..... 13

2.3.2 Extrinsic Semiconductor ..... 13

2.3.2.2 P-type Semiconductor ..... 14

2.3.2.1 N-type Semiconductor ..... 14

2.4 Conductivity of Semiconductor ..... 14
2.4.1 Diffusion Current Density ..... 17
**CHAPTER 3 - PN JUNCTION ..... 18**
3.1 Basic Structure of the PN Junction ..... 18
3.1.1 Electric Field ..... 21
3.1.2 Space Charge Width ..... 23
3.2 PN Junction I–V Characteristic ..... 24
3.2.1 Zener Region ..... 26
**CHAPTER 4 - RADIATION FUNDAMENTALS ..... 28**
4.1 Radiation Energy Terms ..... 28
4.2 Radiation Damage Mechanisms ..... 29
4.2.1 Displacement Damage ..... 29
4.2.2 Ionization Damage ..... 29
4.3 Understanding Traps ..... 30
4.4 Radiation Effects ..... 31
4.5 X-Rays and Gamma Radiations ..... 32
**CHAPTER 5 - EXPERIMENTAL METHOD ..... 33**
5.1 Thermal Evaporation Method ..... 33
5.2 Obtaining Mo/$CuInGaTe_2$/p-Si/Al Diodes ..... 35
5.3 Obtaining of Ohmic Metal Contacts ..... 35
5.4 Linear Accelerator (LINAC) ..... 37
5.5 Bolus ..... 39
5.6 Current-Voltage (I-V) Measurement System ..... 39
5.7 X-Ray Diffraction (XRD) ..... 40

5.8 Scanning Electron Microscopy (SEM)..... 42

**CHAPTER 6 - RESULTS..... 44**

6.1 Characterization of I-V Curves ..... 44

6.2 Determination of Interface States Density ..... 46

6.3 Analysis Results ..... 47

6.4 Discussion and Conclusion ..... 59

**REFERENCES..... 63**

# NOMENCLATURE

## Roman Letter Symbols

| | |
|---|---|
| $A$ | Effective field of diode |
| $A^*$ | Richardson constant |
| $D_n$ | Diffusion coefficient of electrons |
| $D_p$ | Diffusion coefficient of holes |
| $E$ | Electric field |
| $E_c$ | Energy level of conduction band in eV |
| $E_f$ | Fermi energy level |
| $E_g$ | Bandgap of semiconductor in eV |
| $E_v$ | Energy level of valence band in eV |
| $q$ | Charge of electron |
| $I$ | Diode current |
| $I_0$ | Saturation current |
| $J$ | Current density |
| $k$ | Boltzmann constant |
| $n$ | Ideality factor |
| $n_0$ | Number of electrons |
| $n_e$ | Density of electrons |
| $n_i$ | Density of intrinsic carriers |

| | |
|---|---|
| $n_h$ | Density of holes |
| $N_a$ | Acceptor concentration |
| $N_d$ | Donor concentration |
| $p_0$ | Number of holes |
| $R_s$ | Serial resistance |
| T | Temperature in Kelvin |
| $V_{BD}$ | Breakdown voltage |
| $X_n$ | Space charge width in the n-type region |
| $X_p$ | Space charge width in the p-type region |
| W | Space charge width |
| $\varepsilon_s$ | Permittivity of the semiconductor |
| $\mu_n$ | Electron mobility |
| $\mu_p$ | Hole mobility |
| $\sigma$ | Conductivity |
| $\phi_B$ | Electric potential |

**Acronyms**

| | |
|---|---|
| cGy | centiGray |
| CIGTe | Copper-Indium-Gallium-Telluride |
| Cu | Copper |
| Ga | Gallium |
| Ge | Germanium |

| | |
|---|---|
| In | Indium |
| LINAC | Linear Accelerator |
| Mo | Molybdenum |
| Si | Silicon |
| Te | Telluride |

# LIST OF TABLES

**Table 2.1** Portion of the periodic table related to semiconductors ..... 9

**Table 2.2** Semiconductor materials ..... 10

**Table 6.1** The saturation current $I_0$, the ideality factor and the barrier height values according to the radiation variation of the Mo/CuInGaTe$_2$/p-Si/Al structure..... 50

**Table 6.2** The series resistance and the ideality factor parameters calculated from electrical characteristics of the Mo/CuInGaTe$_2$/p-Si/Al structure as a function of testing radiation ..... 52

**Table 6.3** The barrier height and the series resistance parameters calculated from electrical characteristics of the Mo/CuInGaTe$_2$/p-Si/Al structure as a function of testing radiation ..... 54

**Table 6.4** Values of ideality factor, barrier height and series resistance ..... 60

# LIST OF FIGURES

**Figure 2.1** Formation of energy bands for electrons in a Si crystal with a diamond type lattice structure ..... 11

**Figure 2.2** Representation of energy bands ..... 12

**Figure 3.1** The band diagram of a p-n junction at thermal equilibrium (a) electrons and holes in the two halves (b) flow of carriers to equalise the electrochemical potential difference and formation of depletion region ..... 19

**Figure 3.2** Energy-band diagram of a p-n junction in thermal equilibrium ..... 19

**Figure 3.3** The space charge density in a uniformly doped p-n junction assuming the abrupt junction approximation ..... 22

**Figure 3.4** Electric field in the space charge region of a uniformly doped p-n junction ..... 22

**Figure 3.5** Cross-section of a p-n junction ..... 24

**Figure 3.6** Effect of applied bias on p-n junction (with similar doping levels on either side). In thermal equilibrium the Fermi level is constant across the entire structure and the built-in electric field opposes the diffusion of carriers across the junction. The applied bias is assumed to drop almost entirely across the depletion layer and thus the Fermi level becomes separated by $qV_a$. Forward bias reduces the built-in electric field and thus the built-in potential barrier is reduced by $V_a$ as shown. Reverse bias on the other hand increases the built-in electric field and the built-in potential is increased by $V_a$ ..... 25

**Figure 3.7** I-V characteristic of semiconductor diode ..... 26

**Figure 4.1** Carrier trap location ..... 30

**Figure 4.2** Five effects that can occur due to the presence of defects in semiconductor bandgaps ..... 31

**Figure 5.1** Schematic representation of the thermal evaporation system ..... 33

**Figure 5.2** Thermal evaporation system under vacuum ..... 34

**Figure 5.3** A schematic representation of Mo/$CuInGaTe_2$/p-Si/Al diode ..... 35

**Figure 5.4** $CuInGaTe_2$ thin films grown on the p-Si ..... 36

**Figure 5.5** Mask that used to create upper contacts. ..... 37

**Figure 5.6** Mo/$CuInGaTe_2$/p-Si/Al diode appearances after the back and the top metal contacts are formed ..... 37

**Figure 5.7** Elekta synergy linear accelerator radiotherapy device. ..... 38

**Figure 5.8** Bolus ..... 39

**Figure 5.9** Current-voltage (I-V) measurement system ..... 40

**Figure 5.10** Schematic representation of the bragg equation ..... 41

**Figure 5.11** Rigaku Miniflex 600 X-Ray diffraction (XRD) device ..... 42

**Figure 5.12** A simplified schematic diagram of a scanning electron microscope (SEM) ..... 43

**Figure 6.1** The forward bias I–V characteristics in a semi-logarithmic plot of the Mo/$CuInGaTe_2$/p-Si/Al diode at non-radiated and various doses ..... 48

**Figure 6.2** The experimental LnI vs. I plot obtained from the forward bias I-V characteristics of the Mo/$CuInGaTe_2$/p-Si/Al diode at non-radiated and various doses ..... 49

**Figure 6.3** The relation between the barrier height ($\Phi_B$(I-V)) and the ideality factor (n(I-V)) with irradiation ..... 50

**Figure 6.4** dV/dLnI vs. I plot obtained from forward bias of the Mo/$CuInGaTe_2$/p-Si/Al diode at non-radiated and various doses ..... 51

**Figure 6.5** The relation between the series resistance (Rs(dV/dLn(I)-I)) and irradiation dose ..... 52

**Figure 6.6** The experimental H(I) vs. I plot obtained from forward bias of the Mo/$CuInGaTe_2$/p-Si/Al diode at non-radiated and various doses ..... 53

**Figure 6.7** The relation between the barrier height ($\Phi_B$(Cheung)) and the ideality factor (n(Cheung)) with irradiation ..... 54

**Figure 6.8** The relation between the series resistance (Rs(H(I)-I)) and irradiation dose ..... 55

**Figure 6.9** Comparison of n(I-V) and n(Cheung) measurements with changing radiation..... 55

**Figure 6.10** Comparison of $\Phi_B$(I-V) and $\Phi_B$(Cheung) measurements with changing radiation..... 56

**Figure 6.11** Comparison of $R_S$(dV/dLnI-I) and $R_S$(H(I)-I) measurements with changing radiation..... 56

**Figure 6.12** The density of interface states vs. energy distribution profiles of the Mo/$CuInGaTe_2$/p-Si/Al diode ..... 57

**Figure 6.13** Top view SEM result of the $CuInGaTe_2$ thin film..... 58

**Figure 6.14** X-Ray diffraction data of the $CuInGaTe_2$ thin film..... 58

# CHAPTER 1

## INTRODUCTION

The history of semiconductor technology begins with researches on the electrical properties of materials. The properties of negative temperature coefficient of resistance, rectification, and light-sensitivity were discovered at the beginning of the 19th century.

In 1883, Michael Faraday reported that when the silver sulfide was heated, the resistance was falling. This situation is the opposite of the behavior of other metallic substances. In 1839, A.E. Becquerel observed a voltage between a solid and a liquid electrolyte (photovoltaic effect) when light was applied. In 1873, Williough by Smith discovered that the resistance produced by selenium diminished when the light was dropped on them. In 1874, Karl Ferdinand Braun observed current rectification and conductivity properties of metal sulfides. Arthur Schuster saw that the copper oxide layer on the surface of the wires was pointing to the rectifying effect and that this effect was lost when the wires were cleaned. Adams and Day observed photovoltaic effect in selenium in 1876 [1].

A unified description of these incompletely understood events was possible with the development of solid state physics in the first half of the 20th century. In 1878, Edwin Herbert Hall described the Hall Effect, which is also known by its name, that the flowing charge carriers deviate when magnetic field is applied. J.J. Thomson's discovery of electrons in 1897 led to the introduction of electron-based conduction theories. Karl Baedeker, by observing a Hall Effect with the reverse sign to that in metals, theorized that copper iodide had positive charge carriers. In 1914, Johan Koenigberger classified solid materials as metals, insulators and variable conductors. Josef Weiss, a student of Koenigberger, described the semiconducting term in a modern sense in his doctoral dissertation, published in 1910. In 1928, Felix Bloch published a theory of how electrons move in atomic lattice patterns. In 1930, B.

Gudden argued that the conductance in the semiconductors was due to a small amount of impurity. By 1931, "The band theory of conduction" was put forward by Alan Herries Wilson and the concept of band gap was developed. Walter H. Schottky and Nevill Francis Mott improved models of the potential barrier and of the characteristics of a metal-semiconductor junction. In 1938, Boris Davydov brought the theory of copper-oxide rectifier to the world of science, describing the p-n junction and describing the importance of minority carriers and surface states [2].

Despite all the struggles, in some cases the experiments gave rather irrelevant results than the theoretical prediction. The reason for these conclusions can be understood by John Bardeen's explanation that the extremed "structure sensitive" behavior of semiconductors, whose properties alter dramatically rely on tiny amounts of impurities [2]. Materials which were known to be pure in the 1920s containing varying proportions of trace contaminants produced differing experimental results. This has been an important result for the development of improved material research techniques. Nowadays, with modern methods, semiconductors can be produced that do not contain more than parts-per-trillion purity of impurities.

Prior devices containing semiconductors were produced with reference to experimental data. Once the semiconductor theory was developed, more useful and reliable devices have begun to be produced. In 1880, Alexander Graham Bell used the selenium's light sensitivity feature to transmit a sound over a beam of light. In 1883, Charles Fritts produced a low-yield solar cell by using a metal plate coated with selenium and a thin layer of gold. In the 1930s, this solar cell was used commercially as photographic light meter [2]. In 1904, lead sulfide point-contact microwave rectifiers were produced by Jagadish Chandra Bose. Cat-Whisker Detectors, produced from natural galena or other materials, have been widely used in the development of radio. However, some things still can not be predicted more precisely and require some adjustments. In 1906, H.J. Round discovered that when the current flowed through the silicon carbide crystals that form the basis of the LED, they lighted. Oleg Losev observed the publication of a similar light in 1922, but at that time it was not a practical

application. Current rectifiers including copper oxide and selenium were produced in the 1920s and became commercially important as an alternative to vacuum tube rectifiers [1, 2].

In the years prior to World War II, research on infrared detection and communication technologies led to the concentration of lead sulphide and lead selenide materials. These devices were used to locate the vessels and aircraft, and for voice communicate. Point-of-contact crystal detectors became vital for microwave radio systems. Because the existing vacuum tube devices did not work as detectors at 4000 MHz level. For this reason, advanced radar systems have been produced using crystal detectors that provide high-speed response. Significant research and development of silicon materials occured during the war to develop detectors of consistent quality [2]. Detectors and current rectifiers could not be used to amplify the signal. As the theoretical knowledge about semiconductors is rather limited, many studies and researches were unsuccessful in order to develop solid state signal amplifiers [2]. In 1922 Oleg Losev succeeded in producing two terminal and negative resistance amplifiers for radio. In 1926, Julius Edgar Lilienfeld patented a device that resembled a field-effect transistor, although it could not be used practically. R. Hilsch and R. W. Pohl produced a solid state amplifier in 1938, which resembles the control structure of vacuum tubes. Although this device seems to be power saving, it has a limit frequency and its practical application is very limited. But it was still important in terms of being an effective application of the existing theory [2]. In 1938 at Bell Laboratories, William Shockley and A. Holden began working on solid state amplifiers. The first silicon p-n junction was observed in 1941 with a sample with sharp differences between the p and n regions in terms of light sensitivity. A thin slice from the sample at the p–n boundary produced a potential difference when exposed to light.

During the war in France, Herbert Matare observed amplification between adjacent point contacts on a germanium base. After the war, Matare's research group announced their "Transistorn" amplifier announced after Bell Laboratories announcing the “transistor”.

## 1.1 A General View of Semiconductor Materials

Research on semiconducting materials started in the early 19th century. Since then, many semiconductors have been investigated. Certainly, the most well-known materials are Silicon (Si) and Germanium (Ge), which both belong to column IV of the periodic table of elements. While a bulk crystal of Si or Ge consists of the periodic arrangement of a single atom, other semiconductors like gallium arsenide (GaAs) are built with two different elements: Ga(III) and As(V). Such composite semiconductors have electrical or optical properties that are not achievable with pure semiconductors made of only one type of atom.

Before the bipolar transistor was invented in 1947, semiconductors were used in basically two types of electrical devices: photodiodes and rectifiers. In the 1950s, Ge used to be the most frequently employed material. However, it could not be used in applications requiring weak current consumption and operation under high temperatures. Si has started overcome all other semiconductors since 1960, because it was both significantly cheaper and less power consuming [3].

Radiation damage to materials is a topical and wide field of study in modern science. Study of radiation effects on electronic components is a very important segment of this field, because one already can hardly imagine a world without various electronic devices for ordinary life, scientific or military purposes. Moreover, Si-based technology has proven to be relatively sensitive to radiation [4].

Radiation effects on electronics were first observed during above-ground nuclear bomb tests in 1954 [5]. Spurious signals and malfunctions of the measuring equipment were observed. During nuclear explosion, most of the energy is released in form of neutrons, gamma rays, alpha particles and electrons. Temporary errors in electronics or so called single event effects (SEEs) were mainly caused by neutrons, while gammas were responsible for permanent effects like modification of characteristics of electronic components [6]. Since 1958, similar anomalies were registered in electronic devices operating in space.

In recent years, the use of diode dosimeters has become very common in radiation therapy. Various researchers have presented methods for measuring the input and output of the diode detectors to determine the dose to the median plane. The principle of the diode dosimetry system method is based on the phenomenon of the semiconductor p-n junction and detection of radiation [7].

## 1.2 Review of Related Works

Thin films are important because of the applicability capacities in many areas of the industry. The thickness of thin films ranges from a few atoms to 100 μm (<100 nm or 0.001 μm). Thin films should have appropriate thickness, composition and characteristic properties to show the expected functions. In industries, thin films are used as high-tech materials that are interested in optical, electronic, magnetic, chemical and mechanical fields because they have many features that they can not provide by itself when they are coated on the surface of bulky materials. In addition, they can be used as electronic circuit elements because they behave like new materials, when they are multi-layered, completely different from their volume characteristics. The past decade, such work has mainly focused on binary ($In_2S_3$, CdS), ternary ($CuInSe_2$, AgGaSe2) and quaternary ($CuInGaSe_2$) films. Recently, there have been few reports on the synthesis of quinary ($CuInGa(Se_{(1-x)}Te_x)_2$) films [8-11].

Fiat et al. [9] have studied effect of stoichiometry and annealing on optical and structural properties of $CuIn_{0.7}Ga_{0.3}(Se_{(1-x)}Te_x)_2$ chalcopyrite thin films. They found that Te rich films have more beneficial effect on the grain structure, optical properties and device performance.

In another study, Fiat et al. [10] have investigated the annealing temperature and stoichiometry effect on the properties of CuInGaSe and CuInGaTe chalcopyrite thin films. The films have been prepared by the electron bean evaporation technique. They found that all films grown on glass substrates have been found to indicate a better crystallinity at higher annealing temperatures, but the Se substitution by Te led to a slight degradation of their quality.

Jaber Al-Ta'ii et al. [12] have studied the effect of alpha radiation on the current-voltage characteristics of Al/DNA/p-Si/Al Schottky diodes. These diodes were exposed to radiation for different durations (2, 4, 6, 8, 10 and 20 minutes) and various diode parameters such as ideal factor, barrier height, series resistance and saturation current were calculated from the I-V data obtained at each irradiation. It has been observed that the ideality factor is greater than one in the calculations. This shows that there is an effect of another current-carrying mechanism besides thermionic emission on the diode. It was also observed that there was an increase in the series resistance values with the increase of the irradiation time.

Teffahi et al. [13] have investigated effect of gamma radiation on the electrical properties of Ti/Au/$GaAs_{1-x}N_x$ Schottky diodes. I-V measurements at room temperature are used to study 50 kGy $^{60}$Co γ-ray electrical properties irradiation dependence of Ti/Au/$GaAs_{1-x}N_x$ Schottky diodes. The forward bias I–V measurements indicate that thermionic emission is the dominant transport mechanism. Ideality factor increased after irradiation because of recombination current and series resistance effects. The density of interface states increased with radiation due to irradiation-induced defect. The series resistance increase with irradiation due to γ-ray irradiation produce traps levels and recombination centers that reduce relaxation time.

In another study, Rao et al. [14] have investigated effect of 8 MeV electron irradiation on the electrical characteristics of Au/n-Si Schottky diodes. A decrease in the value of barrier height and increase in the ideality factor are observed with increase in electron dose. Irradiation might have introduced defects at the Au/n-Si interface leading to the reduction in Schottky barrier height. This has been interpreted as a result of defects in the Au/n-Si interface, which caused the beam to decrease in the Schottky barrier height.

Taşcıoğlu et al. [15] have studied radiation effect on the Al/SiO/p-Si (MIS) structures from the forward bias *I–V* characteristics before and after $^{60}$Co gamma-ray irradiation. The Al/SiO/p-Si (MIS) structures were irradiated with $^{60}$Co gamma-ray source in the

dose range of 0–5 kGy. The Nss values revealed an experimental decrease with increasing bias from the top of the valance band towards the mid gap.

Baran et al. [16] have investigated the effects of gamma radiation on the electrical characteristics of metal organic semiconductor (MOS) capacitor. The values of Nss decreases with the increasing radiation dose. The results demonstrated that the electrical properties of the MOS capacitor depend on gamma radiation.

## 1.3 Aim of the Study

The purpose of this study is to examine the effect of X-Ray radiation on the normal functionality of the $CuInGaTe_2$ semiconductor diode. The electronic parameters of diode were investigated by current-voltage (I-V) measurements. The diode was exposed for different doses (200, 400, 600, 800 and 1000 cGy) of irradiation. The various electrical parameters such as ideality factor, barrier height and series resistance were determined from forward bias I-V measurement method and Cheung's functions. Measurements were performed under 6 MV X-Ray beams by a linear accelerator (LINAC) and field sizes of $10\times10$ $cm^2$ is used, shaped by standard applicators.

The forward bias current measurements as functions of applied voltage characteristics of the pre-radiated and irradiated samples were performed using a Keithley 2400 sourcemeter. The current was measured from 0 Volt to +1 Volt applied bias. Before and after irradiation, the I-V measurement of diodes were carried out at room temperature in darkness. 6 MV X-Ray beam was used to irradiate the samples in the direction normal to the sample.

In this work, we demonstrated the effect of ionizing X-Ray irradiation on a $CuInGaTe_2$ semiconductor diode by investigating its current-voltage characteristics. The junction obtained shows a non-ohmic and rectifying character [17].

This thesis is organized into six chapters. First chapter contains an introduction to semiconductors, related works and the purpose of the study. In the second and third chapters, theoretical basics of semiconductors and p-n junction were given. The fourth

chapter describes radiation fundamentals and gives general subject matter information regarding radiation induced effects on semiconductive characteristics. Chapter five, “Experimental Method” section includes test system and describes how the $CuInGaTe_2$ structure is formed. In the last chapter, chapter six, the experimental results of the study were compared and discussed.

# CHAPTER 2

## SEMICONDUCTORS

### 2.1 Introduction

Semiconductors are a group of materials having conductivities between those of metals and insulators. The conductivity of a semiconductor is generally sensitive to temperature, illumination, magnetic field, and minute amounts of impurity atoms. This sensitivity in conductivity makes the semiconductor one of the most important materials for electronic applications. Semiconductors are classified as elemental and compound semiconductor materials. The elemental semiconductor materials, found in group IV of the periodic table, and the compound semiconductor materials mostly consist of special combinations of the III and V group elements.

#### 2.1.1 Element Semiconductors

The element semiconductors, those composed of single species of atoms, such as Si and Ge, can be found in column IV. Table 2.1 shows a portion of the periodic table related to semiconductors.

**Table 2.1** Portion of the periodic table related to semiconductors.

| **Period** | **Column** | | | | |
|---|---|---|---|---|---|
| | **II** | **III** | **IV** | **V** | **VI** |
| **2** | | B | C | N | O |
| **3** | Mg | Al | Si | P | S |
| **4** | Zn | Ga | Ge | As | Se |
| **5** | Cd | In | Sn | Sb | Te |
| **6** | Hg | | Pb | | |

### 2.1.2 Compound Semiconductors

The two-element, or binary, compounds such as gallium arsenide or gallium phosphide are formed by combining one group III and one group V element. The important compound semiconductors as well as the two-element-semiconductors are listed in Table 2.2.

Three element or triple compound semiconductors can also be formed. An example is $Al_xGa_{1-x}As$, in which the subscript x indicates the fraction of the lower atomic number element component. More complicated semiconductors can be formed that provide flexibility when selecting material properties [18, 19].

**Table 2.2** Semiconductor materials.

| **General Classification** | **Semiconductor** | |
|---|---|---|
| | **Symbol** | **Name** |
| **Element** | Si | Silicon |
| | Ge | Germanium |
| **Binary compound** | SiC | Silicon carbide |
| | GaAs | Gallium arsenide |
| | InP | Indium phosphide |
| | CdTe | Cadmium telluride |
| | $CuInTe_2$ | Copper indium telluride |
| | $AgGaTe_2$ | Silver gallium telluride |
| **Triple compound** | $Al_xGa_{1-x}As$ | Aluminum gallium arsenide |
| | $Ga_{1-x}In_xAs$ | Gallium indium arsenide |
| | $Ga_xIn_{1-x}N$ | Gallium indium nitride |
| **Quaternary compound** | $CuIn_xGa_{1-x}Te_2$ | Copper indium gallium telluride |
| | $Al_xGa_{1-x}As_xSb_{1-x}$ | Aluminum gallium arsenic antimonide |
| | $Ga_xIn_{1-x}As_{1-x}P_x$ | Aluminum indium arsenic phosphide |

## 2.2 Energy Bands

According to the Bohr atomic model, in an isolated atom, the energy of any of its electrons is decided by the orbit in which it revolves. But when two identical atoms are brought closer together, the quantized energy levels hybridize and split into two different levels because of the mutual interaction of the two atoms. More generally, when N atoms are moved closer, until they reach the equilibrium inter-atomic distance d, the energy levels split into N levels. These N levels are very close to each other if N is large (which is the case in a crystal) so that they eventually form a continuous energy band.

Consider an isolated Si atom; its energy levels are quantized. Si atoms arranged in a periodic lattice, but with a very large lattice parameter (or inter-atomic distance), in order to first consider that each atom as isolated. The two levels with the highest energy are labeled $E_1$ and $E_2$. Now let's shrink homothetically the atom lattice: Energy levels split and form two continuous bands known as the conduction band (CB) and the valence band (VB), Figure 2.1 shows the formation of these bands as a function of the inter-atomic distance.

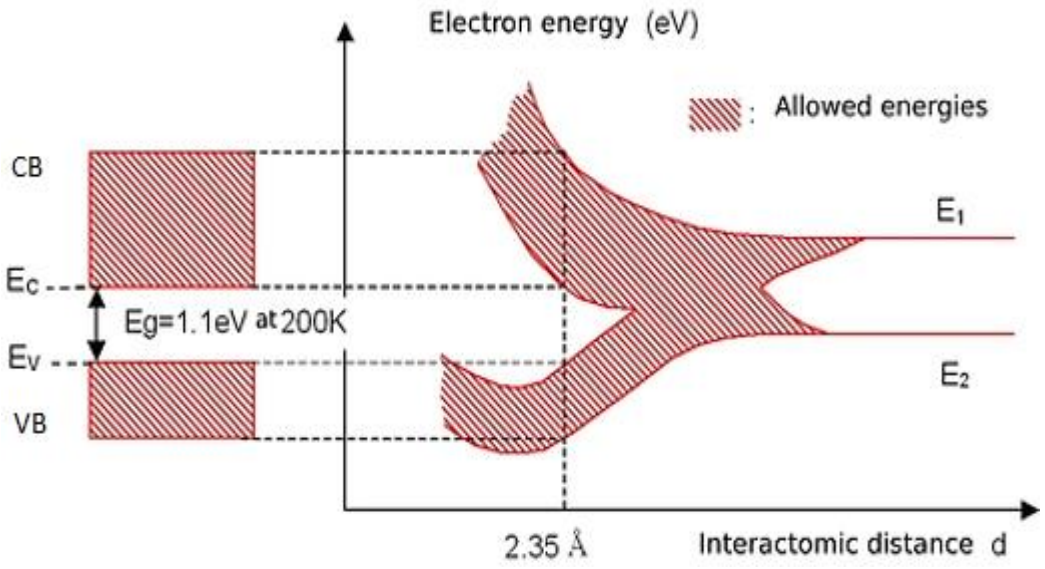


**Figure 2.1** Formation of energy bands for electrons in a Si crystal with a diamond type lattice structure.

In a Si crystal ($d_0 = 2.35\ \text{A}^{\circ}$), two continuous energy bands exist (CB and VB), separated by a forbidden band, which is not accessible for electrons. This forbidden region is called the "gap" and its width $E_g$ is a characteristic of the material. The lowest energy level of the CB is denoted $E_C$ and the highest energy level of the VB is called $E_v$ so that we have the relationship $E_g=E_c-E_v$. The CB and VB represent the energies accessible to electrons, or the energies of the states potentially occupied by electrons: they do not provide any information about the effective occupation of the energy states by electrons.

## 2.3 Insulator, Semiconductor, Conductor

The electrical properties of a given material depend on the electronic populations of the different allowed bands. Electric conduction occurs as a result of the movement of electrons in the bands. When an electric field is applied to the material, the electrons start to move in the opposite direction of the electric field. An empty energy band and a fully occupied band do not participate in the formation of an electric current. Indeed, an electron can move provided that, whenever it leaves its site, it can find some free space elsewhere (another available site within its energy band, called a "hole"), where it can go. Representation of energy bands is given Figure 2.2. In an insulator, the CB is empty, but the VB is fully occupied. Insulators have a large band gap. In this case the VB (and all bands of lower energy) is totally occupied, and the CB is empty.

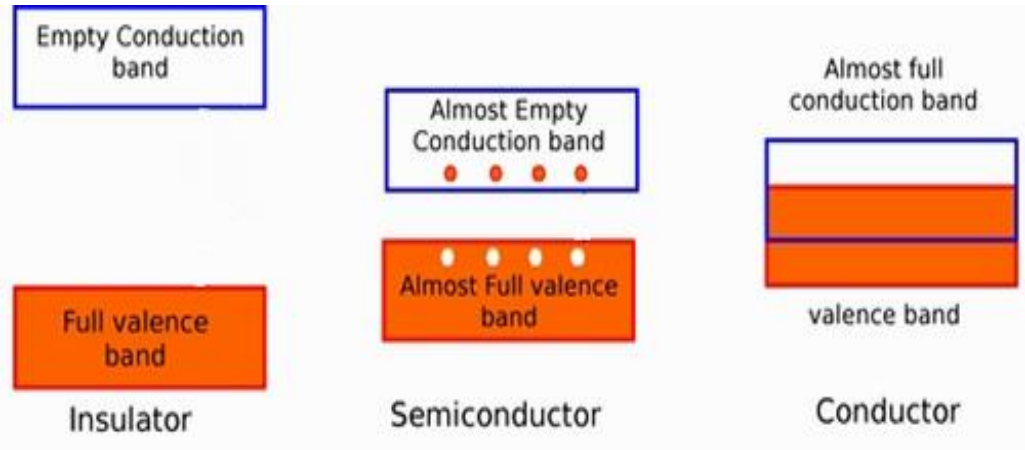


**Figure 2.2** Representation of energy bands.

A semiconductor is initially an insulator at 0K. However, since the energy gap is lower compared to insulators (~1eV), the VB is slightly thermally populated at room temperature, whereas the CB is slightly depopulated. Since electrical conduction is directly connected to the number of electrons in the "almost empty" CB and to the number of holes in the "almost fully occupied" VB, it can be expected that the electrical conductivity of such an intrinsic semiconductor will be very small.

For a conductor, CB and VB are not separated and there is therefore no energy gap. The CB is then partially occupied (even at low temperatures), resulting in a "high" electrical conductivity [3].

### 2.3.1 Intrinsic Semiconductors

A pure semiconductor which is free from every impurity is called intrinsic semiconductor. Ge and Si are the important examples of intrinsic semiconductors.

In intrinsic semiconductor:

$$n_e = n_h = n_i \tag{2.1}$$

where $n_e$, $n_h$ are number density of electrons in CB and number density of holes in VB, $n_i$ is the number density of intrinsic carriers in a pure semiconductor.

Doping: It is a process of deliberate addition of a desirable impurity to a pure semiconductor to modify its properties in a controlled manner. The impurity atoms added are called dopants. The impurity added may be ≈ 1 in $10^{10}$ atoms.

### 2.3.2 Extrinsic Semiconductor

A doped semiconductor or a semiconductor with suitable impurity atoms added to it is called extrinsic semiconductor. Extrinsic semiconductors can be classified in two types.

#### 2.3.2.2 P-type Semiconductor

When a pure semiconductor of Ge or Si is doped with a controlled amount of trivalent atoms, say indium or boron or aluminum, P-type semiconductor or acceptor type semiconductor is obtained. It is called P-type because the conduction of electricity in such semiconductor is due to motion of holes. It is called acceptor type because the doped impurity atom creates a hole in semiconductor which accepts the electron resulting conduction in P-type semiconductor [20].

#### 2.3.2.1 N-type Semiconductor

When a pure semiconductor of Ge or Si is doped with a controlled amount of pentavalent atoms, say arsenic or phosphorus or antimony or bismuth, N-type semiconductor or donor type semiconductor is obtained. It is called N-type semiconductor, because the conduction of electricity in such semiconductor is due to motion of electrons or N-type carriers. It is called donor type, because the doped impurity atom donates one free electron to semiconductor for conduction.

## 2.4 Conductivity of Semiconductor

In a pure semiconductor, the number of holes is equal to the number of electrons. Thermal agitation continues to produce new electron-hole pairs and the electron-hole pair disappears because of recombination. With each electron-hole pair created, two charge-carrying particles are formed. One is negative which is the free electron with mobility $\mu_e$. The other is positive, i.e. the hole with mobility $\mu_h$ [21].

The application of an external electric field induces a drift of the charge carriers; the mobility can then be alternatively defined as the ratio between the velocity,$V_d$, of the charges and the amplitude of the applied electric field, E:

$$\mu = \frac{V_d}{E} \tag{2.2}$$

Here $V_d$ is the drift velocity.

The average velocity that an electron or hole achieved due to the applied voltage or electric field is called drift velocity. The ability of an electron to move through a metal or semiconductor, in the presence of applied electric field is called electron mobility [22, 23].

The mobility of the conductive band is mathematically written as:

$$\mu_e = \frac{q\tau_e}{m_e^*} \tag{2.3}$$

where q is charge of an electron. $\tau_e$, $m_e^*$ are mean free time between collisions for electron and effective mass of electron.

The mobility of the VB is mathematically written as:

$$\mu_h = \frac{q\tau_h}{m_h^*} \tag{2.4}$$

Here $\tau_h$, $m_h^*$ are mean free time between collisions for hole and effective mass of hole.

Since each electron carries a charge -q**,** the net electron current density J, due to the electric field will be:

$$J_e = qn_0\mu_e E \tag{2.5}$$

where $J_e$ is drift current density due to free electrons and $n_0$ is number of electrons.

The hole current density due to the electric field will be:

$$J_h = qp_0\mu_h E \tag{2.6}$$

where $J_h$ is drift current density due to holes and $p_0$ is number of holes.

The electrons and holes move in opposite directions in an electric field E, but since they are of opposite sign, the current due to each is in the same direction. Hence the total current density J is the sum of the hole and electron current densities:

$$J = J_e + J_h \tag{2.7}$$

$$J = q(n_0\mu_e + p_0\mu_h)E \tag{2.8}$$

This current is called the drift current density. The quantity $q(n_0\mu_e + p_0\mu_h)$ is called the conductivity and is given the symbol σ. The units of conductivity are siemens per centimeter, S/cm. Thus, we can write:

$$J = \sigma E \tag{2.9}$$

The inverse of the conductivity is called the resistivity ρ**:**

$$\rho = \frac{1}{\sigma} \tag{2.10}$$

The units of resistivity are ohm-centimeters, Ω.cm.

It is evident from the above equation that current density within a semiconductor is directly proportional to the applied electric field.

For pure (intrinsic) semiconductor, $n = p = n_i$, where $n_i$ is the intrinsic carrier concentration.

Therefore,

$$J = n_i(\mu_e + \mu_h)qE \tag{2.11}$$

and conductivity of an intrinsic semiconductor is $\sigma_i = qn_i(\mu_e + \mu_h)$. Hence it is clear that conductivity of an intrinsic semiconductor depends upon its intrinsic concentration ($n_i$) and the mobility of electrons ($\mu_e$) and holes ($\mu_h$). The intrinsic conductivity of Ge and Si increase by approximately 5% per $^0$C and 7% per $^0$C rise in temperature respectively due to the influence of $n_i$.

Conductivity of N-type and P-type semiconductors: The conductivity of an intrinsic semiconductor:

$$\sigma_i = qn_i(\mu_e + \mu_h) = q(n\mu_e + p\mu_h) \tag{2.12}$$

For N-type semiconductor, as e≫h, then the conductivity:

$$\sigma = qn\mu_e \tag{2.13}$$

For P-type semiconductor, as h≫e, then the conductivity [21]:

$$\sigma = qp\mu_h \tag{2.14}$$

### 2.4.1 Diffusion Current Density

Diffusion is the net motion of carriers in a concentration gradient. This motion results from the continual random thermal motion of the carriers [24].

Hole diffusion current density:

$$J_h^{diff} = -qD_h \frac{\partial p}{\partial x} \tag{2.15}$$

Electron diffusion current density:

$$J_e^{diff} = qD_e \frac{\partial n}{\partial x} \tag{2.16}$$

where $D_h$, $D_e$ are the diffusion coefficient of holes and the diffusion coefficient of electrons. The total electron and hole current densities are the sum of the respective drift and diffusion current densities:

$$J_h = J_h^{drift} + J_h^{diff} \tag{2.17}$$

$$J_h = qp\mu_h E - qD_h \frac{\partial p}{\partial x} \tag{2.18}$$

and

$$J_e = J_e^{drift} + J_e^{diff} \tag{2.19}$$

$$J_e = qn\mu_e E + qD_e \frac{\partial n}{\partial x} \tag{2.20}$$

$$J_{tot} = J_h + J_e \tag{2.21}$$

Here the total current density $J_{tot}$ is the sum of the electron and hole current densities.

# CHAPTER 3

## PN JUNCTION

### 3.1 Basic Structure of the PN Junction

Figure 3.1 outlines how a p-n junction is formed by bringing together the p-type and the n-type regions and also outlines the energy levels and a junction barrier [25]. When a p-type and n-type materials are placed in contact with each other, the junction behaves very differently than either type of material alone, and it is termed the p-n junction, as shown in Figure 3.1 (a-b). When the p-n junction is formed, some of the electrons in the n-region diffuse across the junction and combine with the holes to form negative ions. A hole can be treated as a particle with a positive mass and a positive charge that is exactly equal in absolute value to an electron, this is depicted by the yellow and the red circles in Figure 3.1 (b). The n-region contains positive donors and a large amount of electrons, while the p-region contains negative acceptors and positive holes. The n-region contains more free electrons, which diffuse to the p-region while the holes in the p-region migrate to the n-region. The flow of carrier from one region of higher concentration to lower concentration results in a diffusion current.

If these particles had no charge, the diffusion process would stop once their concentration becomes equal and no electric field would exists because there will be no electrostatic attraction between them. However due to their opposite charge and the distance between them, an electric field is established and the drift current causes the carriers to flow in the opposite direction to that of the diffusion current.

While in thermal equilibrium no external voltage is applied between the n-type and p-type material, there is an internal potential, which is caused by the work function difference between the n-type and p-type semiconductors. This potential equals the built-in potential, $eV_D$ [26].

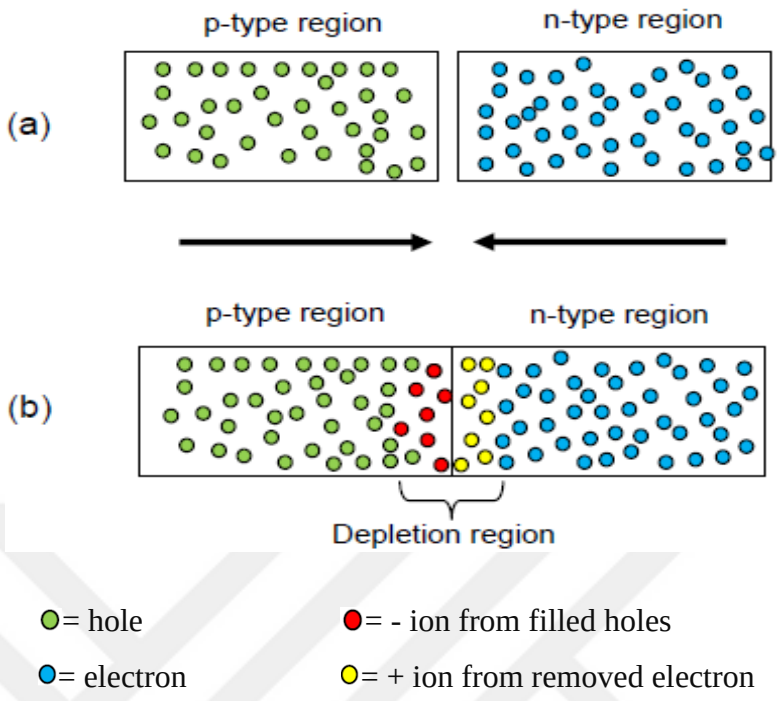


**Figure 3.1** The band diagram of a p-n junction at thermal equilibrium (a) electrons and holes in the two halves (b) flow of carriers to equalise the electrochemical potential difference and formation of depletion region [27].

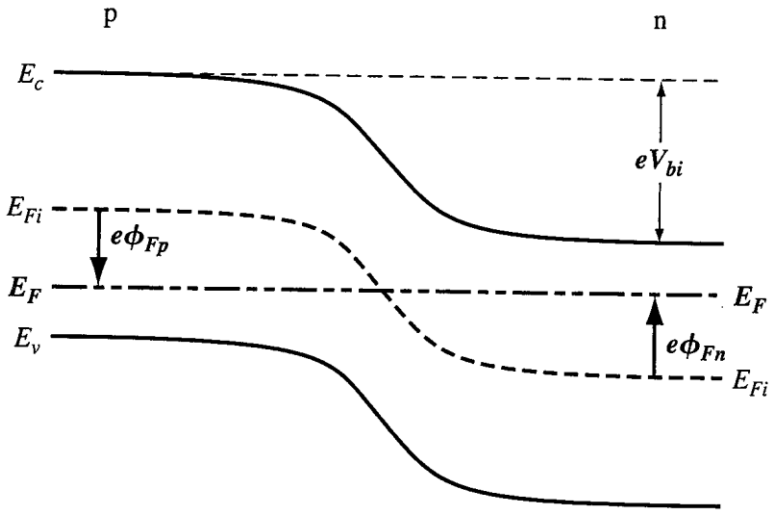


E : Energy at the bottom of the CB — $E_F$: Fermi energy

$E_V$: Energy at the top of the VB — $E_{Fi}$: Intrinsic Fermi level

**Figure 3.2** Energy-band diagram of a p-n junction in thermal equilibrium.

Figure 3.2 reveals the energy band diagram of the p-n junction in thermal equilibrium. The Fermi energy level is constant throughout the entire system. The CB and VB energies must bend as we go through the space charge region, since the relative position of the CB and VB with respect to the Fermi energy changes between p and n regions.

The intrinsic Fermi level is equidistant from the conduction band edge through the junction; thus, the built-in potential barrier can be determined as the difference between the intrinsic Fermi levels in the p and n regions. The potentials $\Phi_{Fn}$ and $\Phi_{Fp}$ can be defined as shown in Figure 3.2, so we have:

$$V_{bi} = |\phi_{Fn}| + |\phi_{Fp}| \tag{3.1}$$

In the n region, the electron concentration in the CB is given by:

$$n_0 = N_d = n_i \exp\left[\frac{(E_F - E_{Fi})}{kT}\right] \tag{3.2}$$

where $N_d$, $n_i$ and $E_{Fi}$ are the donor concentration, the intrinsic carrier concentration and the intrinsic Fermi energy, respectively. K is Boltzman constant and T is absolute temperature.

The potential $\Phi_{Fn}$ in the n region can be defined as:

$$e\Phi_{Fn} = E_{Fi} - E_F \tag{3.3}$$

Equation **(3.2)** may then be written as:

$$n_0 = n_i \exp\left[\frac{-(e\Phi_{Fn})}{kT}\right] \tag{3.4}$$

Taking the natural log of both sides of Equation **(3.4)**, setting $n_0 = N_d$, and solving for the potential:

$$\Phi_{Fn} = \frac{-kT}{e} \ln\left(\frac{N_d}{ni}\right) \tag{3.5}$$

The hole concentration in the p region is given by:

$$p_0 = N_a = n_i \exp\left[\frac{E_{Fi} - E_F}{kT}\right] \tag{3.5}$$

where Na is the acceptor concentration. The potential $\Phi_{Fp}$ in the p region can be defined as:

$$e\Phi_{Fp} = E_{Fi} - E_F \tag{3.6}$$

Combining Equations **(3.5)** and **(3.6)**:

$$\Phi_{Fp} = \frac{kT}{e} \ln\left(\frac{N_a}{n_i}\right) \tag{3.7}$$

Finally, the built-in potential barrier for the step junction is found by substituting Equations **(3.5)** and **(3.7)** into Equation **(3.1)**, which yields:

$$V_{bi} = \frac{kT}{e} \ln\left(\frac{N_a N_d}{n_i^2}\right) = V_t \ln\left[\frac{N_a N_d}{n_i^2}\right] \tag{3.8}$$

Where $V_t = kT/e$ and is defined as the thermal voltage.

### 3.1.1 Electric Field

An electric field is created in the depletion region by the separation of positive and negative space charge densities. The electric field is determined from Poisson's equation, which, for a one-dimensional analysis, is:

$$\frac{d^2\Phi(x)}{dx^2} = \frac{-\rho(x)}{\varepsilon_s} = -\frac{dE(x)}{dx} \tag{3.9}$$

where Φ(x), E(x) and ρ(x) are the electric potential, the electric field, and the volume charge density, respectively. $\varepsilon_s$ is the permittivity of the semiconductor. When this poisson equation is solved, the electric field:

$$E = \frac{-eN_a}{\varepsilon_s}(x + x_p) \qquad -x_p \leq x \leq o \tag{3.10}$$

$$E = \frac{-eN_d}{\varepsilon_s}(x_n - x) \qquad 0 \leq \mathrm{x} \leq \mathrm{x_n} \tag{3.11}$$

The electric field is also continuous at the metallurgical junction, or at x = 0. Setting Equations **(3.10)** and **(3.11)** equal to each other at x = 0 gives:

$$\mathrm{N_a x_p} = \mathrm{N_d x_n} \tag{3.12}$$

Equation **(3.12)** states that the number of negative charges per unit area in the p region is equal to the number of positive charges per unit area in the n region.

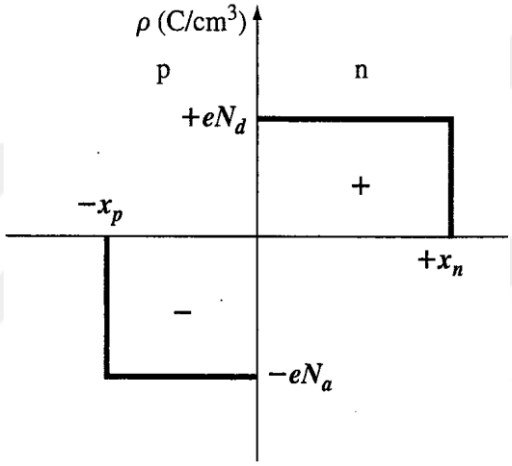


**Figure 3.3** The space charge density in a uniformly doped p-n junction assuming the abrupt junction approximation.

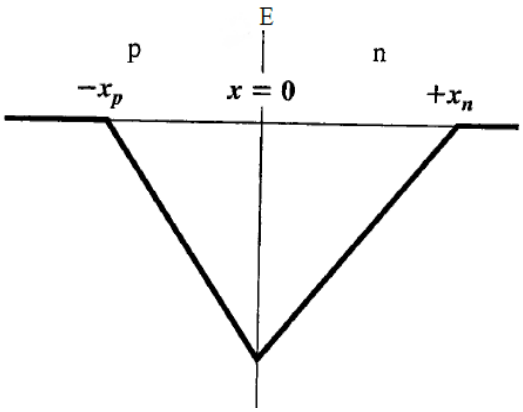


**Figure 3.4** Electric field in the space charge region of a uniformly doped p-n junction [18].

### 3.1.2 Space Charge Width

We can determine the distance that the space charge region extends into the p and n regions from the metallurgical junction. This distance is known as the space charge width.

The space charge width in the n-type region is given by:

$$x_n = \left\{\frac{2\varepsilon_s V_{bi}}{e}\left[\frac{N_a}{N_d}\right]\left[\frac{1}{N_a+N_d}\right]\right\}^{1/2} \tag{3.13}$$

The space charge width into the p-type region is given by:

$$x_p = \left\{\frac{2\varepsilon_s V_{bi}}{e}\left[\frac{N_d}{N_a}\right]\left[\frac{1}{N_a+N_d}\right]\right\}^{1/2} \tag{3.14}$$

where $x_p$ is the width of the depletion region extending into the p region for the case of zero applied voltage.

The total depletion or space charge width W is the sum of the two components, or:

$$w = x_n + x_p \tag{3.15}$$

Using Equations **(3.13)** and **(3.14)**:

$$w = \left\{\frac{2\varepsilon_s V_{bi}}{e}\left[\frac{N_a+N_d}{N_a N_d}\right]\right\}^{1/2} \tag{3.16}$$

The built-in potential barrier can be determined using Equation **(3.8)**, and then the total with of space charge region is obtained from Equation **(3.16)** [18].

## 3.2 PN Junction I–V Characteristic

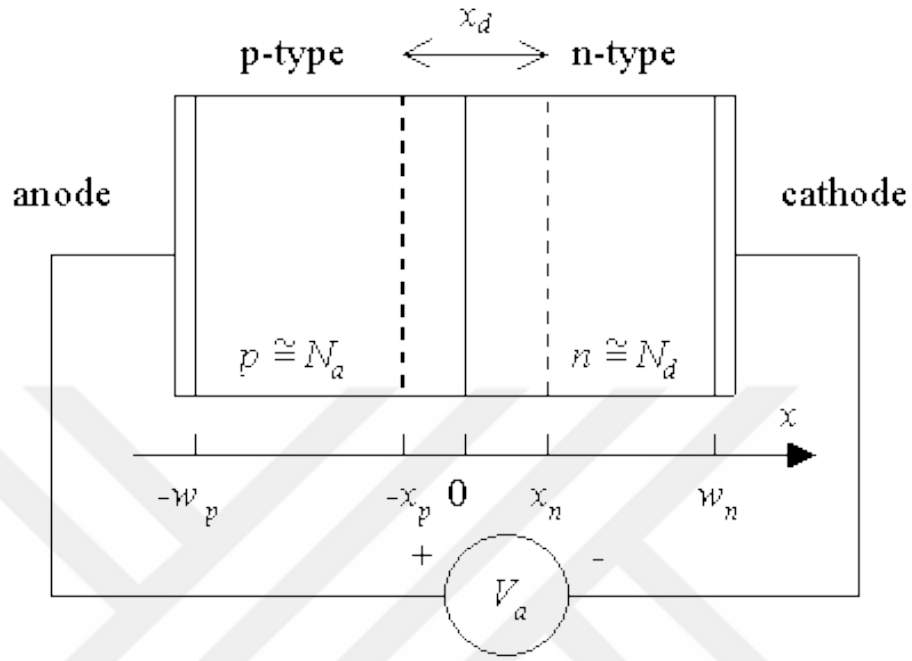


**Figure 3.5** Cross-section of a p-n junction [28].

Assume that the p-n junction is contacted by low-resistance (or ohmic) contacts as illustrated in Figure 3.5. Since the space-charge region is depleted of mobile carriers, the applied voltage, $V_a$, will appear almost entirely across this high-resistance potential barrier region of the junction.

If $V_a$ is positive the built-in voltage will be reduced and the junction is said to be forward biased, whereas if $V_a$ is negative the built-in voltage is increased and the junction is said to be reverse biased. The applied bias will thus alter the barrier to diffusion of carriers across the junction that existed in thermal equilibrium as depicted in Figure 3.6.

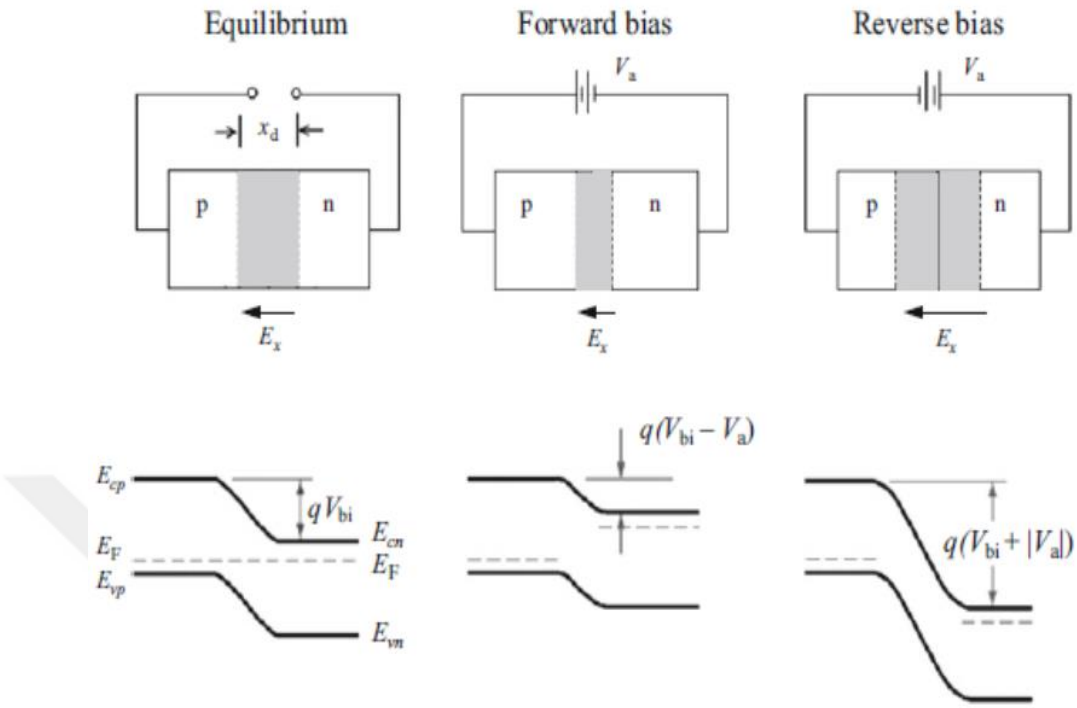


**Figure 3.6** Effect of applied bias on p-n junction (with similar doping levels on either side). In thermal equilibrium the Fermi level is constant across the entire structure and the built-in electric field opposes the diffusion of carriers across the junction. The applied bias is assumed to drop almost entirely across the depletion layer and thus the Fermi level becomes separated by $qV_a$. Forward bias reduces the built-in electric field and thus the built-in potential barrier is reduced by $V_a$ as shown. Reverse bias on the other hand increases the built-in electric field and the built-in potential is increased by $V_a$ [29].

Figure 3.7 summarizes the behavior of the semiconductor diode by means of its I-V characteristic. The reverse breakdown region to the far left of the curve represents the behavior of the diode when a sufficiently high reverse bias is applied. Under such a large reverse bias, the diode conducts current again, this time in the reverse direction. To explain the mechanism of reverse conduction, one needs to visualize the phenomenon of avalanche breakdown. When a very large negative bias is applied to the p-n junction, sufficient energy is imparted to charge carriers that reverse current can flow, well beyond the normal reverse saturation current. In addition, because of

the large electric field, electrons are energized to such levels that if they collide with other charge carriers at a lower energy level, some of their energy is transferred to the carriers with lower energy, and these can now contribute to the reverse conduction process, as well. This process is called impact ionization. Now, these new carriers may also have enough energy to energize other low-energy electrons by impact ionization, so that once a sufficiently high reverse bias is provided, this process of conduction takes place very much like an avalanche: a single electron can ionize several others.

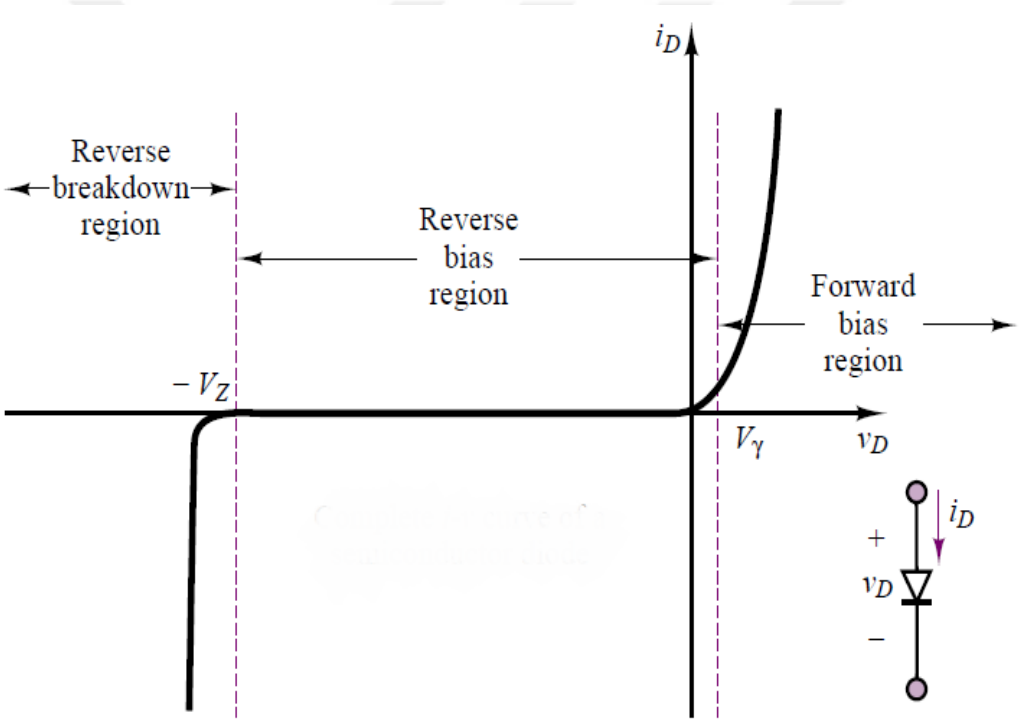


**Figure 3.7** I-V characteristic of semiconductor diode.

### 3.2.1 Zener Region

The phenomenon of Zener breakdown is related to avalanche breakdown. It is usually achieved by means of heavily doped regions in the neighborhood of the metal-semiconductor junction (the ohmic contact). The high density of charge carriers

provides the means for a substantial reverse breakdown current to be sustained, at a nearly constant reverse bias, the Zener voltage, $V_Z$. To summarize the behavior of the semiconductor diode, it is useful to refer to the sketch of Figure 3.7, observing that when the voltage across the diode, $V_D$, is greater than the offset voltage, $V\gamma$, the diode is said to be forward-biased and acts nearly as a short circuit, readily conducting current. When $V_D$ is between $V\gamma$ and the Zener breakdown voltage, $-V_Z$, the diode acts very much like an open circuit, conducting a small reverse current, $I_0$, of the order of only nanoamperes (nA). Finally, if the voltage $V_D$ is more negative than the Zener voltage, $-V_Z$, the diode conducts again, this time in the reverse direction [30].

# CHAPTER 4

## RADIATION FUNDAMENTALS

Radiation is the transmission of energy in the form of electromagnetic waves or particles. It is also possible to define this energy according to the location in the electromagnetic spectrum. Radiation includes, but is not limited to, X-Rays, gamma rays, ultraviolet rays, visible rays, infrared rays, microwaves, and radio waves.

According to quantum mechanics, electromagnetic radiation consists of photons traveling at the speed of light. Gamma and X-Rays from these are radiation with ionizing effect. Gamma rays are emitted from the atomic nucleus, while X-Rays are emitted from the interactions in the orbits outside the nucleus [31, 32].

In general, semiconductor devices are vulnerable to radiation damage because they are radiation sensitive. In these devices, radiation damage occurs primarily through the formation of traps that reduce the lifetimes of minority carriers in the energy band gap. The type of radiation is important in the investigation of degradation in electronic devices. The source of this particle or electromagnetic waves may be nuclear reactions, particle accelerators or natural radiation environment. Different types of radiation can interact in variety of ways with semiconductors [31].

### 4.1 Radiation Energy Terms

To understand the list of radiation levels and exposure rates, the following terms are defined as follows [33]:

| | |
|---|---|
| eV | $1.6\times10^{-19}$ J |
| keV | $10^{3}$ eV |
| MeV | $10^{6}$ eV |
| GeV | $10^{9}$ eV |

| | |
|---|---|
| Dose rate | The rate energy is delivered or absorbed. |
| Flux | Flux defines the number of photons or particles passing through a given area in a specified time. |
| Fluence | Particle fluence is defined as the number of particles traversing a unit area in a unit period of time. |

## 4.2 Radiation Damage Mechanisms

Two basic radiation damage mechanisms can affect semiconductor devices which are "Displacement damage" and "Ionization damage".

### 4.2.1 Displacement Damage

In displacement damage mechanism, incident radiation displaces Si atoms from their lattice sites. The resulting defects alter the electronic characteristics of the crystal.

Displacement damage depends on the non-ionizing energy loss, i.e. energy and momentum transfer to lattice atoms, which depends on the mass and energy of the incident quanta. A simple measure as for ionizing radiation is not possible, so that displacement damage must be specified for a specific particle type and energy.

### 4.2.2 Ionization Damage

In ionization damage mechanism, ionization effects depend primarily on the absorbed energy, independent of the type of radiation. At typical incident energies ionization is the dominant absorption mechanism, so that ionization damage can be measured in terms of energy absorption per unit volume, usually expressed in rad or gray (1 rad= 100 erg/g, 1 Gy= 1 J/kg= 100 rad). Since the charge liberated by a given dose depends on the absorber material, the ionizing dose must be referred to a specific absorber, for example 1 rad(Si), 1 rad($SiO_2$), 1 rad(GaAs), or in SI units 1 Gy(Si), etc.

Both mechanisms are important in detectors, transistors and integrated circuits. Hardly a system is immune to either one phenomenon and most are sensitive to both [34, 35].

## 4.3 Understanding Traps

High levels of ionizing radiation can cause defects in almost all semiconductor devices. Some of these defects reveal trapping energy situations, which correspond to physical recombination sites created within the material's lattice (see Figure 4.1). Trapping energy states are close to the conductivity band edge in the forbidden band gap for donor type traps, and for the acceptor type traps are near the valence band edge inside the forbidden band gap. These traps reduce the lifetime of minority carriers, (τ). The decrease in the lifetime of minority carriers due to trapping in the band gap is defined as follows:

$$\frac{1}{\tau} = \frac{1}{\tau_i} + \frac{\Phi_n}{K} \tag{4.1}$$

where $\tau_i$ is the minority carrier lifetime before irradiated, $\Phi_n$ is the incident neutron fluence, and K is the damage constant. According to Equation **(4.1)**, fluence is proportional to minority carrier lifetime [34].

Looking at Figure 4.1, it can be seen that the traps are located between the valence band and the conduction band, near the band edges in the forbidden energy gap.

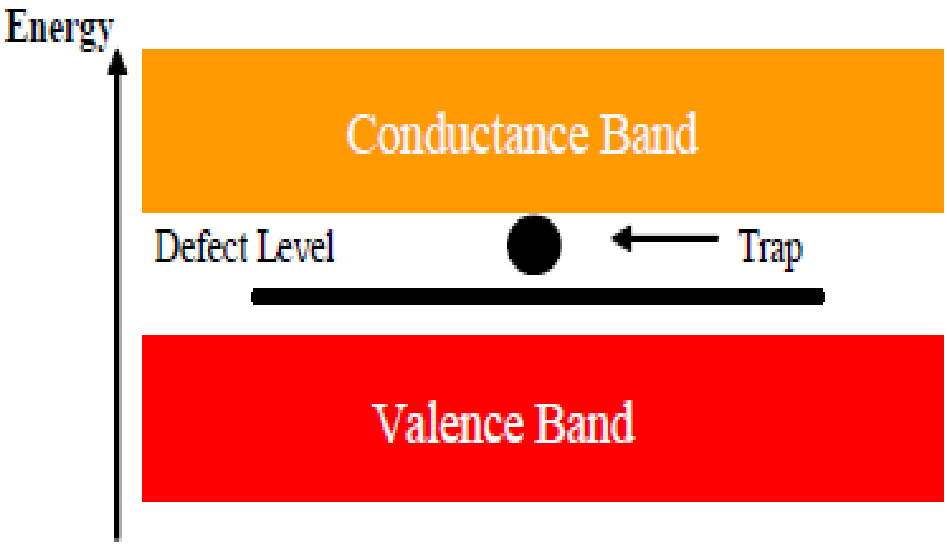


**Figure 4.1** Carrier trap location.

## 4.4 Radiation Effects

When radiation-induced defects begin to affect semiconductor characteristic properties, some defects that may occur within its bandgap. Figure 4.2 shows a variety of defects that may occur in semiconductors.

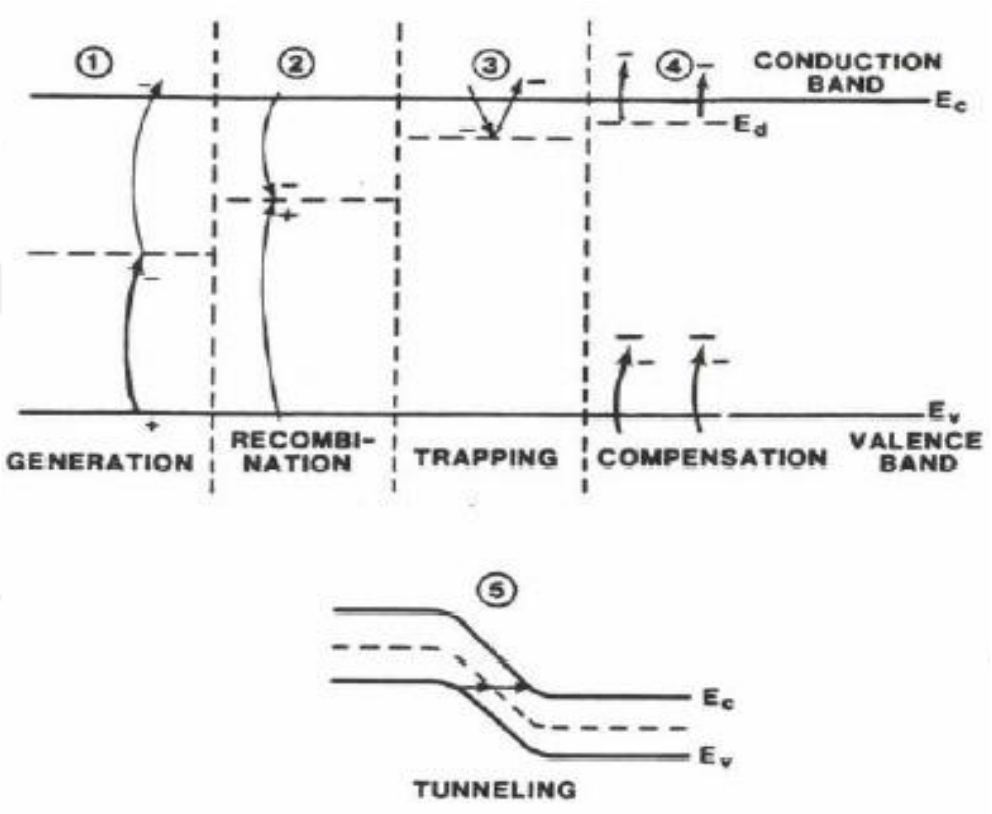


**Figure 4.2** Five effects that can occur due to the presence of defects in semiconductor bandgaps [36].

As the generation creates electron-hole pairs, the recombination annihilates the electron-hole pairs. It is nature's order restoring mechanism, whereby the carrier excess or deficit inside the semiconductor is stabilized or eliminated. The device operation continues until the equilibrium state is reached. However, exposure to the harmful ionizing radiation dose may trigger this process and cause the intended operation of the device to deteriorate. In this regard, generation and recombination are defined as radiation-induced defects.

Other defects that occur as a result of harmful radiation exposure are traps, compensation and tunneling. Traps reduce the carrier lifetime of semiconductors by holding electrons in the energy gap. Compensation allows too many electrons to enter the energy range, causing a reduction in the stability of semiconductor devices.

Finally, tunnelling allows electrons to jump across the energy gap without altering their energy level. This defect can lead the device to be unstable and sometimes cause the device to respond poorly [31, 37].

## 4.5 X-Rays and Gamma Radiations

X-Ray and gamma radiations are formed by electromagnetic radiations; they can interact with matter in three types. 1. Photo Effect; 2. Compton Effect; 3. Pair production. The X-Ray and γ-radiation are extremely shortwave length, the X-Ray is from $10^{-9}$ m to $10^{-12}$ m and γ-radiation is from $10^{-12}$ m to $10^{-14}$ m which finds many important applications in since and medicine. Irradiation has helped agriculture, engineering and industry, and has saved thousands of lives through its medical and biological effects. The p-n junction plays an important role, in both modern electronic applications and semiconductor devices. It is used extensively in rectification, switching and other operations in electronic circuits [38].

# CHAPTER 5

## EXPERIMENTAL METHOD

The $CuInGaTe_2$ crystal used as a source material in the thermal evaporation system is coated on p-Si substrate in the form of thin film and subjected to different radiation values for characterization study.

### 5.1 Thermal Evaporation Method

Thermal evaporation is a thin film coating process in which the evaporation of solid materials by electric current is carried out under high vacuum. Figure 5.1 shows schematic representation of the thermal evaporation system. Solid materials are evaporated and allowed to go directly on the substrate without encountering any obstacles. The particles in the form of steam move up to the substrate and become solid again by sharing a large part of their energy with substrate. In this way, by superimposing the particles can be obtained thin films of the desired thickness.

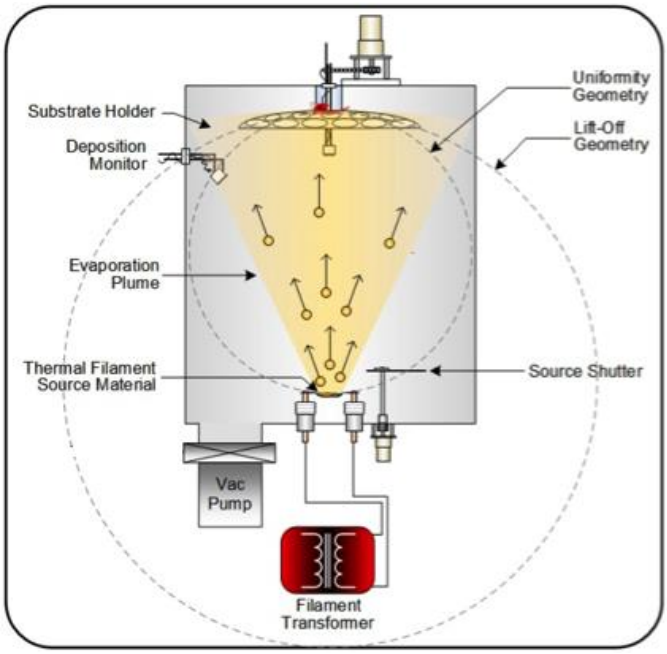


**Figure 5.1** Schematic representation of the thermal evaporation system [39].

Mixed semiconductor crystal, $CuInGaTe_2$ thin films were grown by vacuum evaporation system. In this system, thin films are enlarged in a controlled manner at the desired speed and depending on the computer program. The thickness monitor integrated in the system gives information about the thicknesses of the thin films grown on the substrate by about 20% error.

The Vaksis High Vacuum Evaporation Thin Film Production System, in which $CuInGaTe_2$ thin films investigated in this study is shown in Figure 5.2.




**Figure 5.2** Thermal evaporation system under vacuum.

This process was carried out by cutting the pieces from the mixture crystal at specific weights. The crystals were prepared for evaporation and carefully placed on a molybdenum spoon which had not been used before or was used for the same coating. The p-Si substrate was placed to the holder where the crystals were magnified. Substrate holder hanged about 12 cm above the molybdenum spoon. After this process, the pressure of the vacuum chamber was adjusted to $8x10^{-5}$ torr and the heating was started by passing electric current through the spoon. The enlargement ended when all of the spoon crystals had evaporated.

## 5.2 Obtaining Mo/CuInGaTe$_2$/p-Si/Al Diodes

In this study, the Mo/CuInGaTe$_2$/p-Si/Al diode examined for electrical characteristics. A schematic representation of Mo/CuInGaTe$_2$/p-Si/Al diode is given in Figure 5.3. CuInGaTe$_2$ was grown on (100) oriented p-Si substrate by thermal evaporation system.

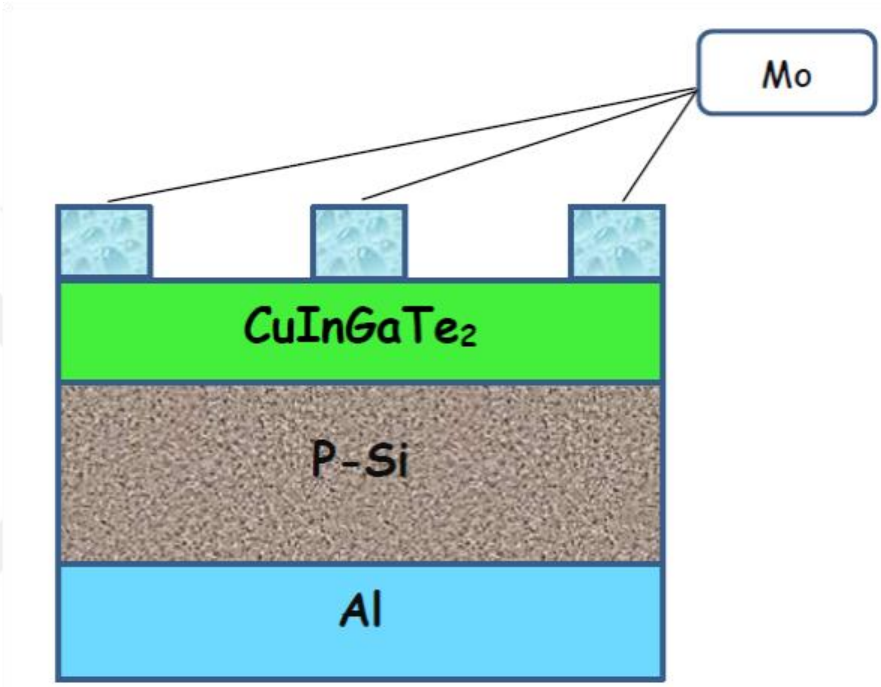


**Figure 5.3** A schematic representation of Mo/CuInGaTe$_2$/p-Si/Al diode.

## 5.3 Obtaining of Ohmic Metal Contacts

First, one surface is dull and the other surface is polished a p-type boron (B) doped Si crystal, which has a [100] orientation and cut off at a thickness of 400 μm was used. The surface of the sample must be free of organic and heavy metal contaminants in order to minimize the occurrence of possible interfacial surface formation and to obtain ideal conditions, it must first be subjected to crystal chemical cleaning to remove organic and heavy metal contamination on the surface.

The crystal dull surface is then selected for the ohmic contact. The p-type Si is coated with 99.9% pure Al metal for the ohmic contact. The heaters used for the evaporation

are cleaned in diluted HF water (HF + $10H_2O$) and dried in deionized water, then rinsed, placed in the coating unit and annealed to remove contaminants. These operations are carried out in a vacuum environment of $10^{-5}$ torr, and the coating medium is supplied air at each time. The metal to be evaporated is thus cleaned.

Following this, the vacuum coating unit is vacuumed and vacuum level is waited until the pressure drops to $10^{-5}$ torr and the Al metal is evaporated by applying current to the heater in the coating unit so that the dull surface of the crystal is covered with metal. Then the sample is taken out by blowing air in vacuum. The temperature of the annealing furnace is set at 575 $^0$C and after the sample is annealed at this temperature for 3 minutes, it is taken out of the annealing furnace to be cooled and waited for cooling. Thus, the ohmic contact of the diode is prepared.

After the ohmic contact was prepared, $CuInGaTe_2$ thin films were grown on the p-Si by vacuum evaporation system as shown in Figure 5.4. Finally, Mo films were sputtered on $CuInGaTe_2$ surface by Magnetron Sputtering method to obtain rectifying contact. To create a rectifying contact, a mask with a 1 mm radial point spacing as shown in Figure 5.5 was placed on the surface of $CuInGaTe_2$/p-Si/Al. At the end of these operations Mo/$CuInGaTe_2$/p-Si/Al diodes were obtained.

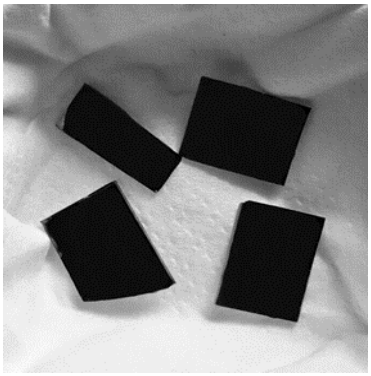

**Figure 5.4** $CuInGaTe_2$ thin films grown on the p-Si.

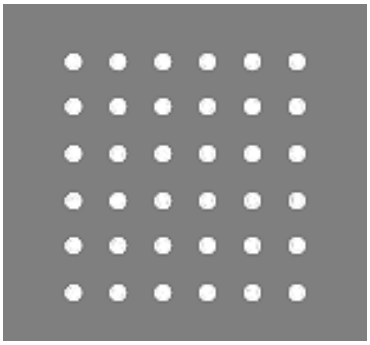

**Figure 5.5** Mask that used to create upper contacts.

The ohmic contacts taken from the back and the top metal contacts are shown in Figure 5.6. Mo/CuInGaTe$_2$/p-Si/Al diodes with ohmic contacts to the back and epitaxial layer were attached with silver paste. In this case, the semiconductor diode is ready for electrical measurement.

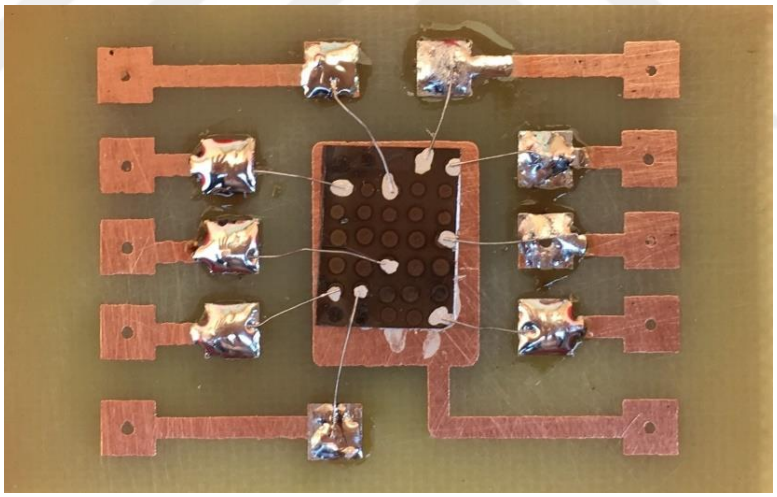

**Figure 5.6** Mo/CuInGaTe$_2$/p-Si/Al diode appearances after the back and the top metal contacts are formed.

## 5.4 Linear Accelerator (LINAC)

Linear accelerators are 6-18 MV X-Rays and 6-18 MeV electron generating devices. Elekta synergy linear accelerator radiotherapy device used in this study is shown in Figure 5.7. LINAC is based on the working principle of an X-Ray tube used to obtain

X-Rays but the distance between the anode and the cathode is longer than that of the X-Ray tube. The electrons emitted from the cathode after reaching very high speeds with a potential in the MV range, and then electrons are hit to the anode (target) and X-Rays are obtained in megavoltage magnitude.

Focus skin length is 100 cm in LINAC and due to the ability to rotate 360 degrees around an axis from the center of the gantry, it allows treatment to be performed in accordance with isocentric techniques. These devices allow larger areas with a higher sharpness (lower penumbra) area to be irradiated at higher energies than Co-60 Teletherapy devices. LINAC offers more opportunities for treatment than Co-60s, but is more expensive and requires more care. LINACs consist of three main parts, electron accelerator, electron deflector and collimator (head) parts [40].

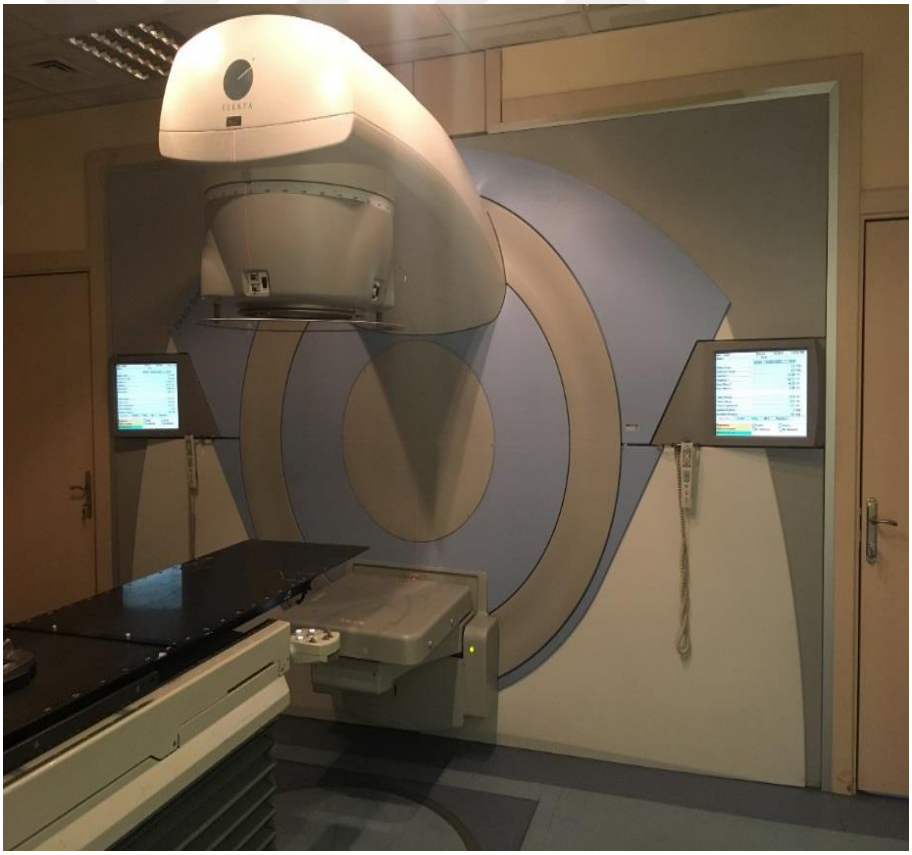

**Figure 5.7** Elekta synergy linear accelerator radiotherapy device.

## 5.5 Bolus

Bolus is a material which has properties equivalent to tissue when irradiated in radiotherapy. It is used to increase the skin dose. It is made from an improved flexible transparent gel (is given Figure 5.8) that adapts to body shapes. In this study, a bolus was used to increase the surface dose while the diodes were irradiated.

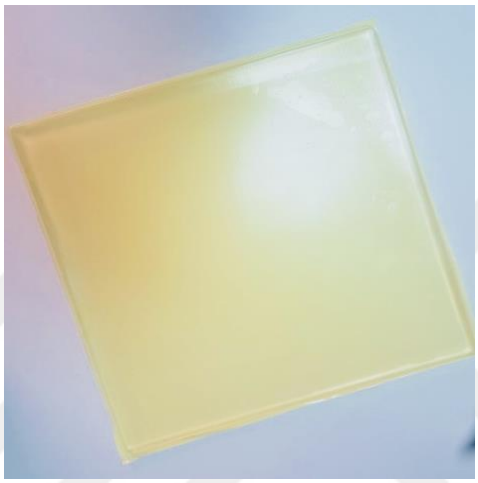

**Figure 5.8** Bolus

## 5.6 Current-Voltage (I-V) Measurement System

The system shown in Figure 5.9 is designed to perform the electrical conductivity measurements of the semiconductor diodes. The Keithley 2400 sourcemeter was used for current-voltage (I-V) measurements of the Mo/CuInGaTe$_2$/p-Si/Al diode. The system is controlled by a computer with a specially prepared program for I-V measurements.

For the analysis of the change of radiation-related electrical parameters, firstly diodes were irradiated with X-Ray at predetermined radiation values (200, 400, 600, 800 and 1000 cGy) and I-V measurements were taken in darkness at each irradiation result.

The data obtained by the measurements allowed the calculation of parameters such as the ideality factor, series resistance, barrier height, and their radiation dependent changes.

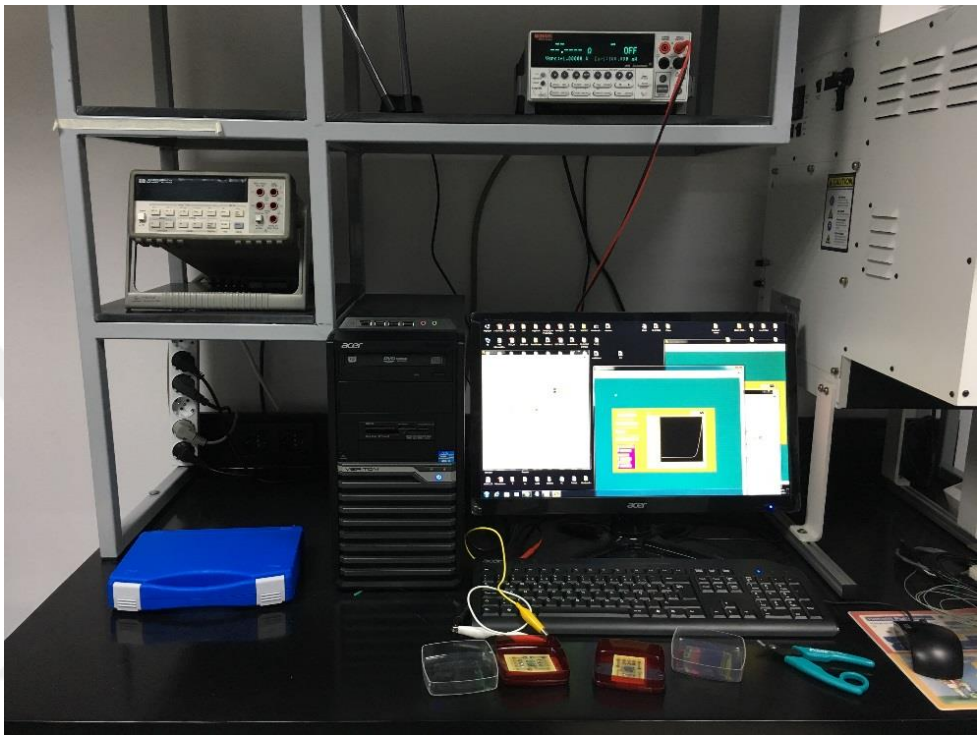

**Figure 5.9** Current-voltage (I-V) measurement system.

## 5.7 X-Ray Diffraction (XRD)

X-Ray diffraction is a powerful characterization technique used in the analysis of crystalline solids. This technique is suitable for thin film analysis, mainly due to two reasons; 1. The wavelengths of X-Rays are in the dimension of atomic distances in condensed matter, and this property allows them to be used in structural investigations. 2. X-Ray diffraction techniques are not destructive and do not alter the sample being examined.

The interatomic distances between the crystal and the molecules are between 0.15 and 0.4 nm. This distance corresponds to the electromagnetic spectrum wavelength of X-rays with photon energies between 3 keV and 8 keV. Therefore, when crystal and

molecular structures are exposed to X-Rays, constructive and destructive interference can be observed.

When X-Rays are directed on a crystal structure, the rays are reflected from the solid surface to the complete reflection at the small incidence angle, and the rays are scattered by the parallel planes of the atoms in the crystal. These scatterings in the crystal structure are called diffraction, and they occur from scattering of a large number of atoms. The diffraction of X-rays in the crystal structure is explained by the Bragg Law and the Bragg law is given by:

$$n\lambda = 2d\mathrm{Sin}\theta \tag{5.1}$$

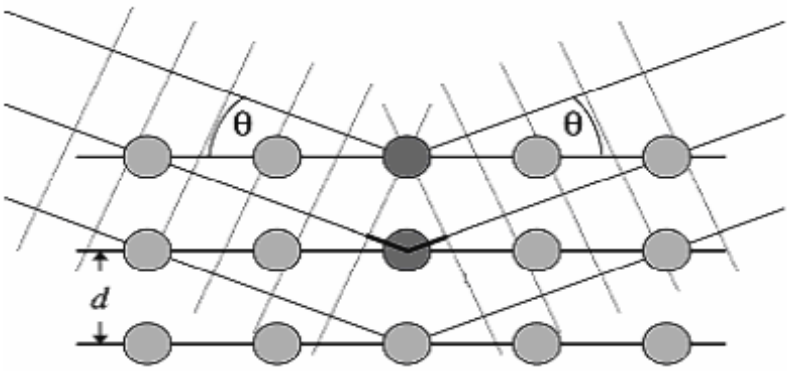


**Figure 5.10** Schematic representation of the bragg equation

Modern X-Ray devices have radiation counters to measure the diffraction angle and intensity of the refracted beam. Thus, the diffraction pattern is obtained which changes the diffraction angle (2Theta) according to the intensity of the diffracted ray. Information on the crystallization of the material can be obtained by looking at the peak widths and intensity of the pattern [41]. In this study, X-Ray analyzes were performed with Rigaku Miniflex 600 X-Ray diffraction (XRD) device (Figure 5.11).




**Figure 5.11** Rigaku Miniflex 600 X-Ray diffraction (XRD) device.

## 5.8 Scanning Electron Microscopy (SEM)

Scanning electron microscopy (SEM) works with the principle of scanning the surface with high-energy electrons that focus on a very small area. The structure of the scanning electron microscope is schematically shown in Figure 5.12. The V-shaped tungsten filament of the electron gun is heated in vacuum to a temperature of about 2800 $^{0}$C. The electrons are released from the tungsten by the thermionic emission and they are pushed through the filament by a negative potential of ~ 30 kV. Electrons passing through the evacuated tube are focused on the sample with the help of electromagnetic lenses (2 or 3) placed around the tube. The most commonly used form of measurement is the measurement of secondary electrons emitted from the surface (SE), especially the image associated with the topographic structure of the surface and the electrons emitted backwards. The vacuum system in SEM is very important, the pressure must be low enough to prevent the operation of the electron gun. It is desirable that the electron emitting surfaces be low to prevent corrosion [42].

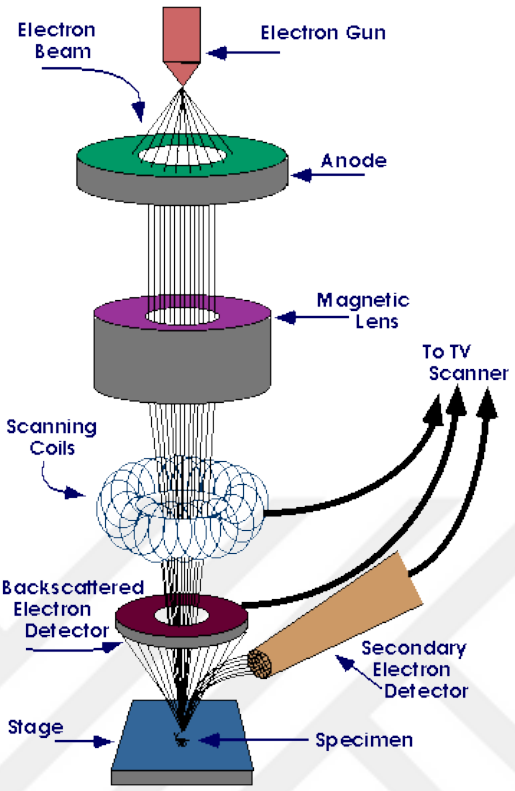


**Figure 5.12** A simplified schematic diagram of a scanning electron microscope (SEM).

# CHAPTER 6

## RESULTS

In this chapter, the electronic parameters of Mo/CuInGaTe$_2$/p-Si/Al diodes exposed to X-Ray radiation at different doses was investigated by current-voltage (I-V) measurements at room temperature in darkness. First, this structure was exposed to different radiation doses and then the saturation current ($I_0$), ideality factor (n), barrier height ($\Phi_B$) and series resistance ($R_S$) were determined from forward bias I-V measurement method and Cheung's functions. In addition, the interface states density (*N*ss) was determined from the forward bias I-V values. By using the I-V characteristics, saturation current, ideality factor, barrier height and series resistance of diode parameters were calculated for all irradiated diodes. These parameters were also calculated by means of Cheung-Cheung's methods and given as comparatively. Measurements are performed under 6 MV X-Ray beams with 200, 400, 600, 800 and 1000 cGy radiation doses by a LINAC.

### 6.1 Characterization of I-V Curves

The forward bias I-V features of a junction, where the series resistor is concerned, can be expressed by the thermionic emission theory:

$$I = I_0 \exp\left(\frac{q(V-IR_s)}{nKT}\right)\left[1-\exp\left(-\frac{q(V-IR_s)}{kT}\right)\right] \quad (6.1)$$

for V>3kT/q can be written as:

$$I = I_0 \exp\left(\frac{qV}{nKT}\right) \quad (6.2)$$

where the electron charge is q, the applied voltage is represented by V, the ideality factor is n, k is the Boltzmann constant, T is the temperature and $I_0$ is the saturation current which can be given as:

$$I_0 = AA^*T^2 \exp\left(\frac{-q\Phi_B}{KT}\right) \quad (6.3)$$

where A, $\Phi_B$ are the effective diode area (A=0,031416cm$^2$), and the zero-bias barrier height. $A^*$ is the effective Richardson constant. In this equation, $I_0$ was obtained by extrapolating the linear region of the LnI-V curve to the LnI axis at the zero voltage.

$\Phi_B$ can be obtained from Equation **(6.3)** as:

$$\Phi_B = \frac{KT}{q} \mathrm{Ln}\left(\frac{AA^*T^2}{I_0}\right) \quad (6.4)$$

The barrier height was calculated based on the y-axis intercepts of the semi-log forward bias I-V plots using Equation **(6.4)**. It should be noted that the barrier height is related to the potential barrier at the interface between the $CuInGaTe_2$/p-Si.

Ideality factor, a parameter which is generally used to measure the deviation of practical diodes from ideal thermionic emission model can be extracted from slope of the linear region of the forward bias LnI-V plot and can be written from Equation **(6.2)**.

$$n = \frac{q}{KT}\left(\frac{dV}{d(\mathrm{LnI})}\right) \quad (6.5)$$

Ideality factor is an important parameter that determines the character of the diode. “n” is a unitless parameter. For an ideal diode n=1 and the diode exhibits non-ideal behavior as n increases from 1, i.e., the value increases.

Figure 6.1 shows the experimental I-V characteristics of our $CuInGaTe_2$ diode at the temperature of 300 K in dark. Since the current curve in forward bias quickly becomes dominated by series resistance and deviates from linearity we used the low forward bias part of I-V characteristics to measure n, $\Phi_B$. Taking natural logarithm of Equation **(6.2)** [43]:

$$\mathrm{LnI} = \mathrm{LnI}_0 + \frac{q}{nKT}V \quad (6.6)$$

The I-V characteristics deviate considerably with the change in ideality factor, due to the effect of series resistance. The series resistance, ideality factor and barrier height, of the diode were also measured using the technique developed by Cheung and Cheung's method [44]:

$$\frac{dV}{d(LnI)} = \frac{nKT}{q} + IR_s \tag{6.7}$$

$$H(I) = V - \left(\frac{KT}{q}\right) Ln\left(\frac{I}{AA^*T^2}\right) \tag{6.8}$$

therefore:

$$H(I) = IR_s + n\Phi_B \tag{6.9}$$

## 6.2 Determination of Interface States Density

In the presence of interfacial states between the interface layer and the semiconductor, the applied voltage dependence of the barrier height is defined by [45]:

$$\frac{d\Phi_e}{dV} = \beta = \left[1 - \frac{1}{n(V)}\right] \tag{6.10}$$

where $\beta$ is the voltage coefficient of the effective barrier height ($\Phi_{e)}$ [46] used in place of the barrier height ($\Phi_{b)}$.

From the forward bias I-V characteristics, the energy density distribution profile of the interfacial states for the Mo/CuInGaTe$_2$/n-Si/Al structure balanced with the semiconductor can be determined. The I-V data corresponds to the voltage-dependent ideality factor (n (V)) and $\Phi_e$. n (V) and $\Phi_e$ are given respectively as follows:

$$n(V) = \frac{q}{kT}\left[\frac{V}{Ln(\frac{I}{I_o})}\right] \tag{6.11}$$

$$\Phi_e = \Phi_{b0} + \beta V = \Phi_{b0} + \left(1 - \frac{1}{n(V)}\right) V \tag{6.12}$$

Card and Rhoderick proposed a method for a metal/semiconductor diode having interface states in equilibrium with the semiconductor. In that case, n(V) becomes greater than unity and is given by [47, 48]:

$$n(V) = 1 + \frac{\delta}{\varepsilon_i}\left[\frac{\varepsilon_s}{W_D} + qN_{ss}(V)\right] \quad (6.13)$$

Here $W_D$ and Nss are the space charge width and the density of the interface states, respectively. Nss equation can be written as:

$$N_{ss} = \frac{1}{q}\left[\frac{\varepsilon_i}{\delta}((n(V) - 1) - \frac{\varepsilon_s}{W_D}\right] \quad (6.14)$$

where δ, $\varepsilon_i$ and $\varepsilon_s$ are the thickness of interfacial layer, the permittivities of the interfacial layer and permittivities of the semiconductor, respectively. $\varepsilon s=11.9\varepsilon_o$ and $\varepsilon_i = 4\varepsilon_o$ for p-type Si. The value of dielectric constant ($\varepsilon_o$) is $8.85x10^{-14}$ F/cm.

In p-type semiconductors, the equation of the energy of the interface states is given by [49]:

$$E_{ss} - E_v = q(\Phi_e - V) \quad (6.15)$$

where Ess and Ev are the energy of interface states and the top of the valance band at the surface of the semiconductor.

## 6.3 Analysis Results

The Mo/CuInGaTe$_2$/p-Si/Al diodes were homogenously irradiated under 200, 400, 600, 800 and 1000 cGy doses with a 6 MV X-Ray radiation source LINAC. The forward bias I-V features pre-irradiated and irradiated diodes were measured and all irradiations had been performed at the room temperature in darkness. The Figure 6.1 shows the forward I–V characteristics in a semi-logarithmic plot of the semiconductor diode before and after X-Ray irradiation.

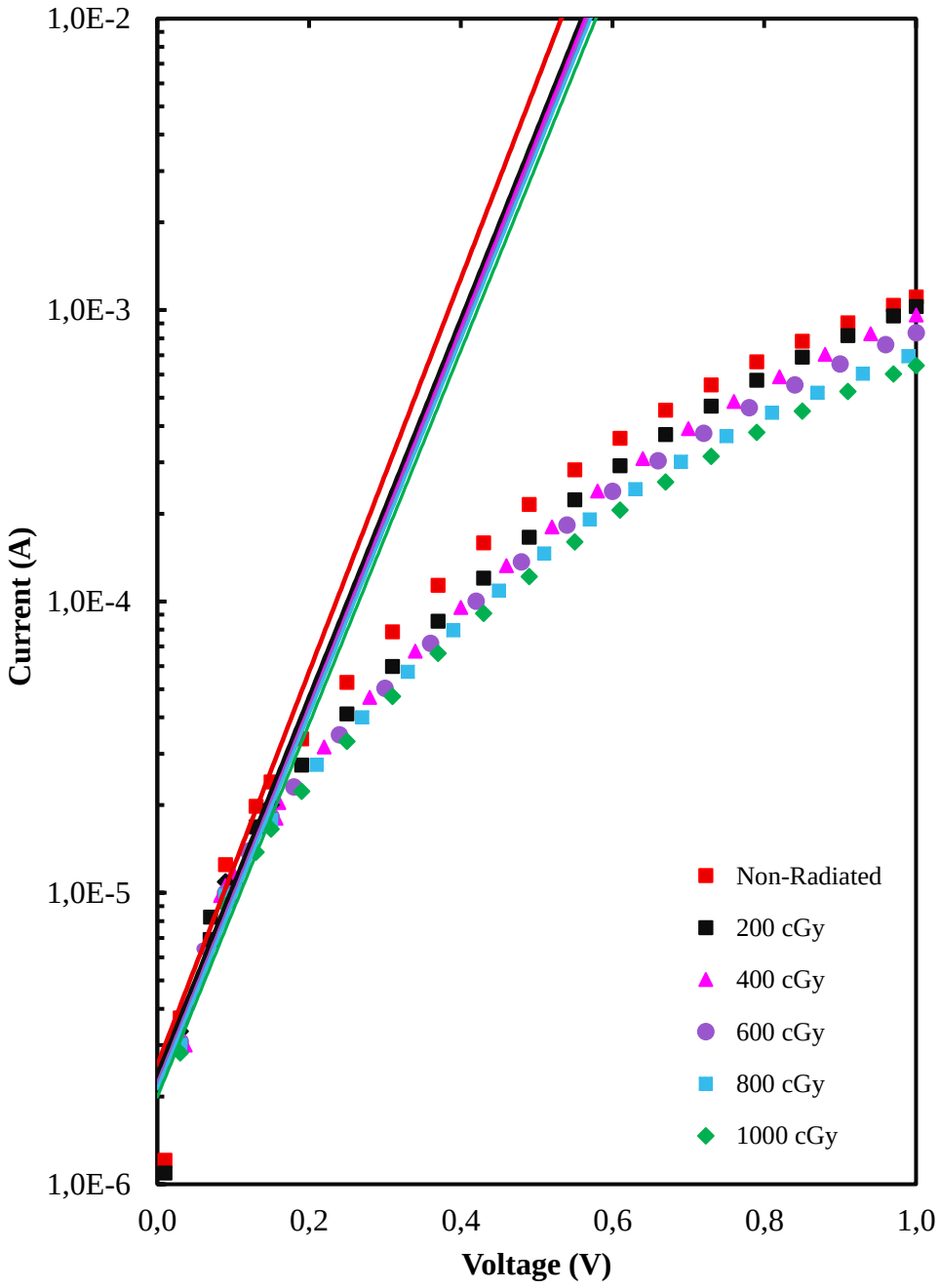


**Figure 6.1** The forward bias I–V characteristics in a semi-logarithmic plot of the Mo/CuInGaTe$_2$/p-Si/Al diode at non-radiated and various doses.

It can be seen from Figure 6.1 that the current-voltage characteristics of the $CuInGaTe_2$ diode is nonlinear and asymmetric. The current curve in the forward bias region becomes dominated by series resistance from contact wires or bulk resistance of the semiconductor diodes, giving rise to the curvature at high current in the semi-logarithmic plot [50].

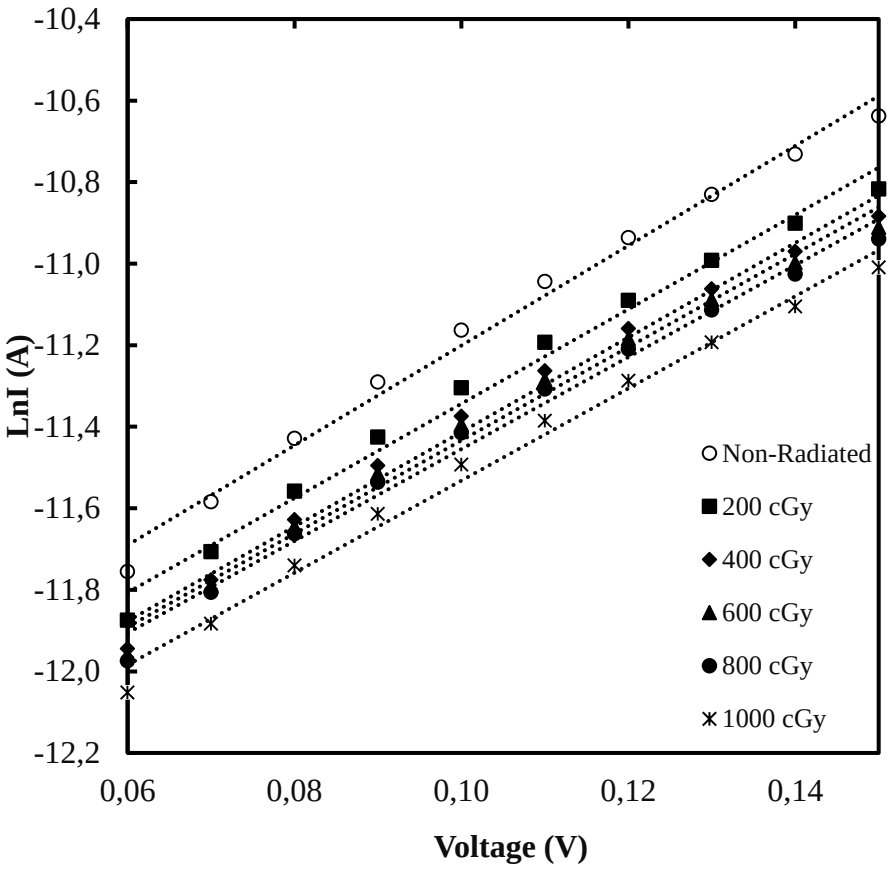


**Figure 6.2** The experimental LnI vs. I plot obtained from the forward bias I-V characteristics of the Mo/$CuInGaTe_2$/p-Si/Al diode at non-radiated and various doses.

The LnI-V graphs of current-voltage data obtained before and after each irradiation were plotted to obtain the slope values of the linear regions. The ideality factor (n) were calculated using Equation **(6.5)**. By fitting the Log (I)-V graphs, the saturation current ($I_0$) values were obtained from the point where the vertical axis was cut at V=0. These values were written in Equation **(6.4)** and barrier heights ($\Phi_B$) were calculated and recorded Table 6.1.

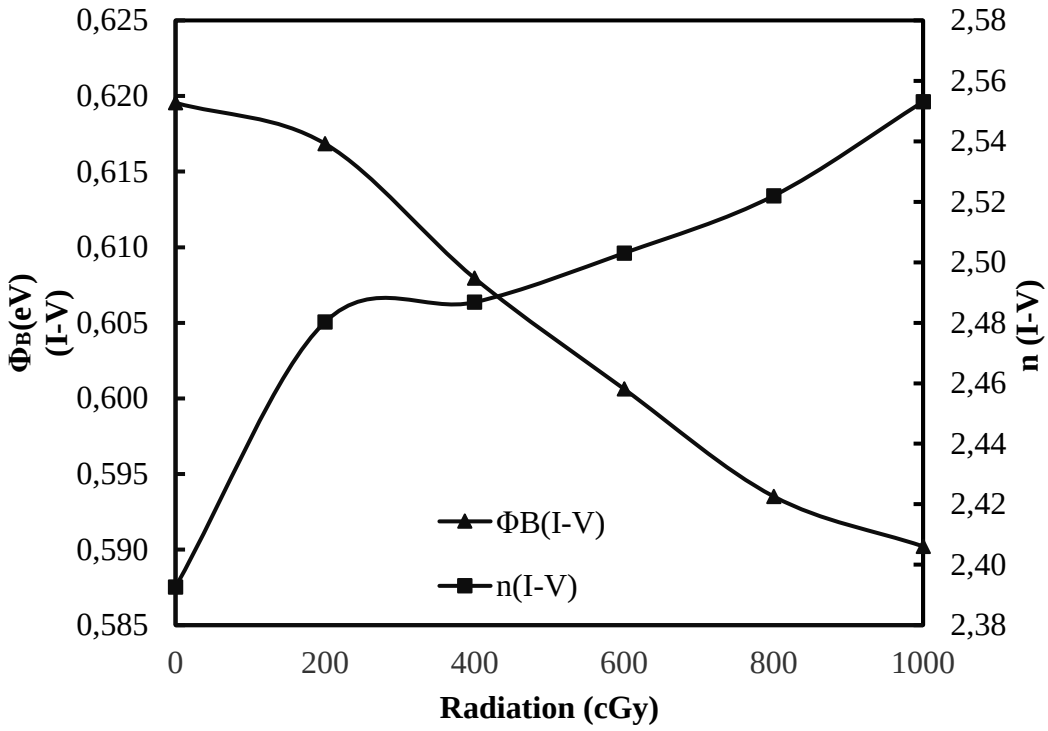


**Figure 6.3** The relation between the barrier height ($\Phi_B$(I-V)) and the ideality factor (n(I-V)) with irradiation.

It was seen from Figure 6.3 that the ideal factor increased and the barrier height decreased with increasing radiation value.

**Table 6.1** The saturation current $I_0$, the ideality factor and the barrier height values according to the radiation variation of the Mo/CuInGaTe$_2$/p-Si/Al structure.

| | I-V | | | | | |
|---|---|---|---|---|---|---|
| **Radiation (cGy)** | 0 | 200 | 400 | 600 | 800 | 1000 |
| **$I_o$(A)** | 4.54E-06 | 4.78E-06 | 4.90E-06 | 5.08E-06 | 5.35E-06 | 5.48E-06 |
| **n** | 2.393 | 2.480 | 2.487 | 2.503 | 2.522 | 2.553 |
| **$\Phi_B$(eV)** | 0.620 | 0.617 | 0.608 | 0.601 | 0.594 | 0.590 |

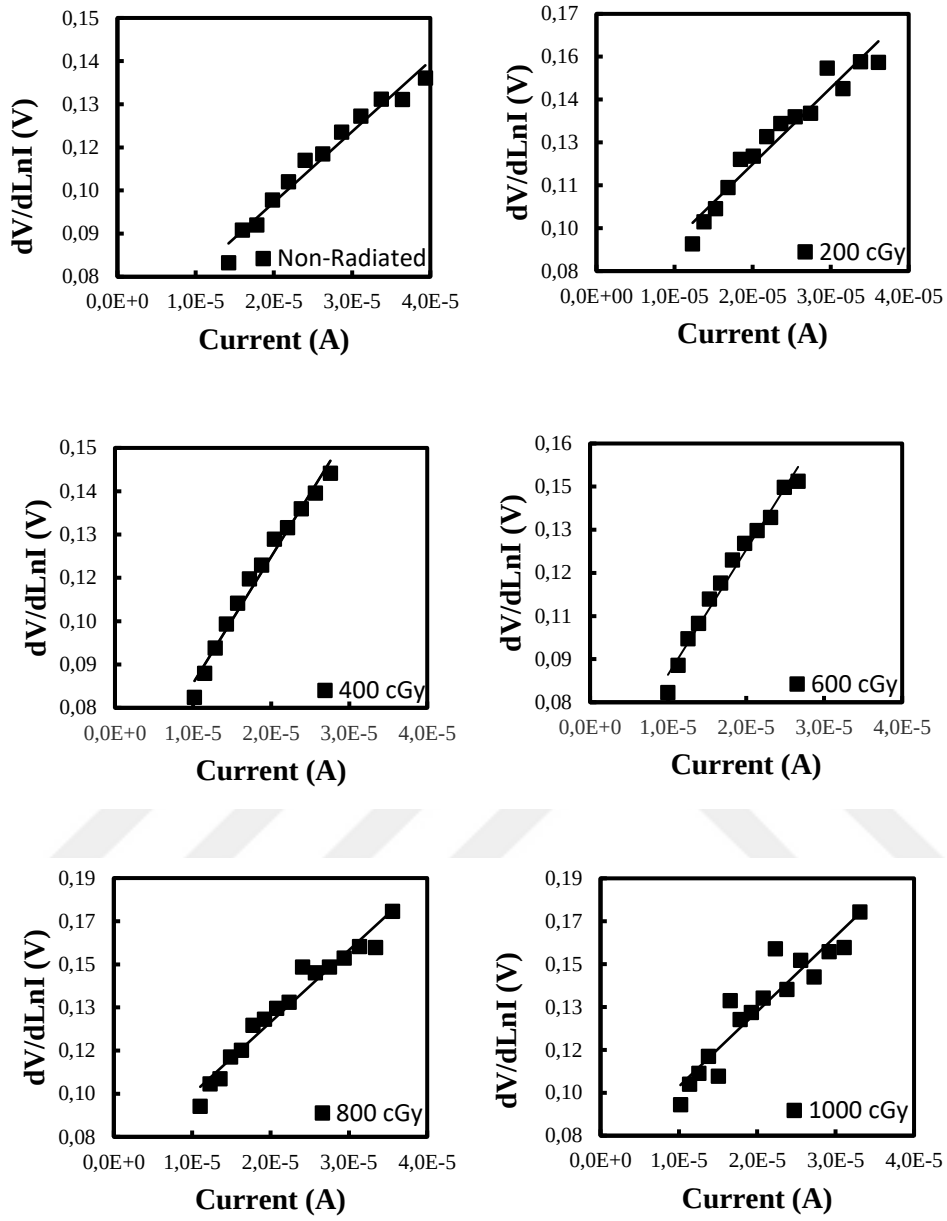


**Figure 6.4** dV/dLnI vs. I plot obtained from forward bias of the Mo/CuInGaTe$_2$/p-Si/Al diode at non-radiated and various doses.

The series resistance was obtained from the slope of the dV/dLnI-I graph, and the ideality factors were calculated from the y-axis cutting point by using Equation **(6.5)**.

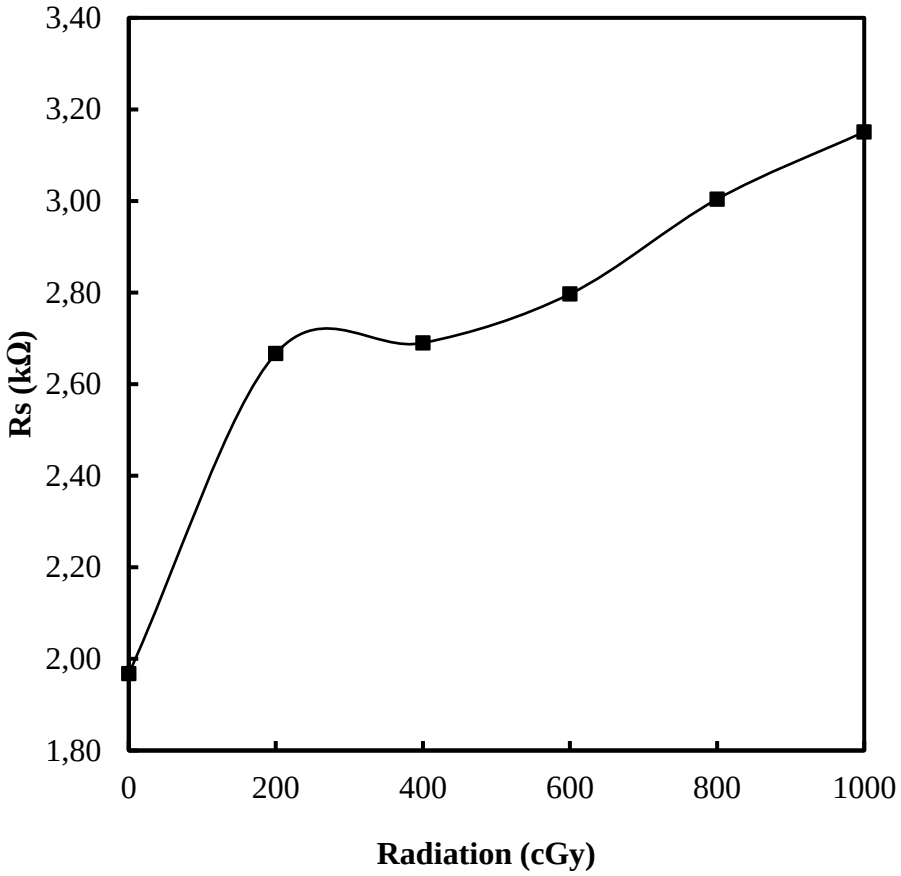


**Figure 6.5** The relation between the series resistance (Rs(dV/dLn(I)-I)) and irradiation dose.

**Table 6.2** The series resistance and the ideality factor parameters calculated from electrical characteristics of the Mo/CuInGaTe$_2$/p-Si/Al structure as a function of testing radiation.

| | dV/dLnI-I (V) | | | | | |
|---|---|---|---|---|---|---|
| **Radiation (cGy)** | 0 | 200 | 400 | 600 | 800 | 1000 |
| **n** | 2.371 | 2.475 | 2.522 | 2.568 | 2.618 | 2.673 |
| **Rs (kΩ)** | 1.968 | 2.667 | 2.690 | 2.797 | 3.004 | 3.151 |

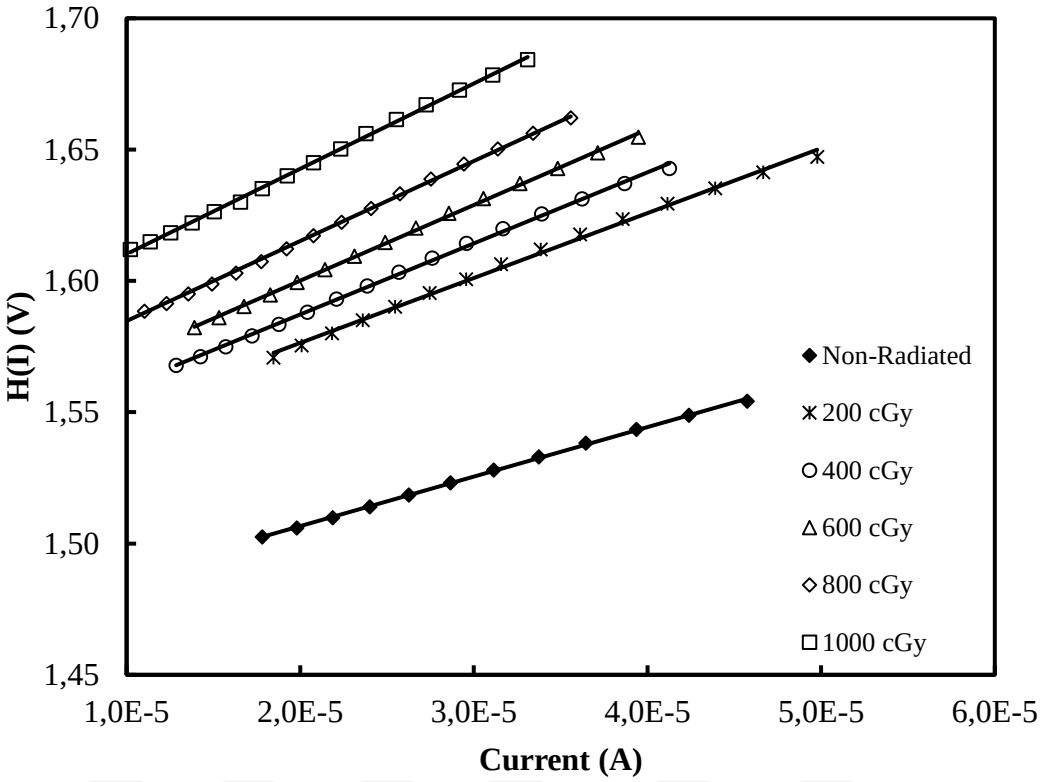


**Figure 6.6** The experimental H(I) vs. I plot obtained from forward bias of the Mo/CuInGaTe$_2$/p-Si/Al diode at non-radiated and various doses.

The series resistance was determined from the slope of the graph H(I)-I and the barrier heights were obtained using Equation **(6.9)** from the point at which the H(I) axis was cut.

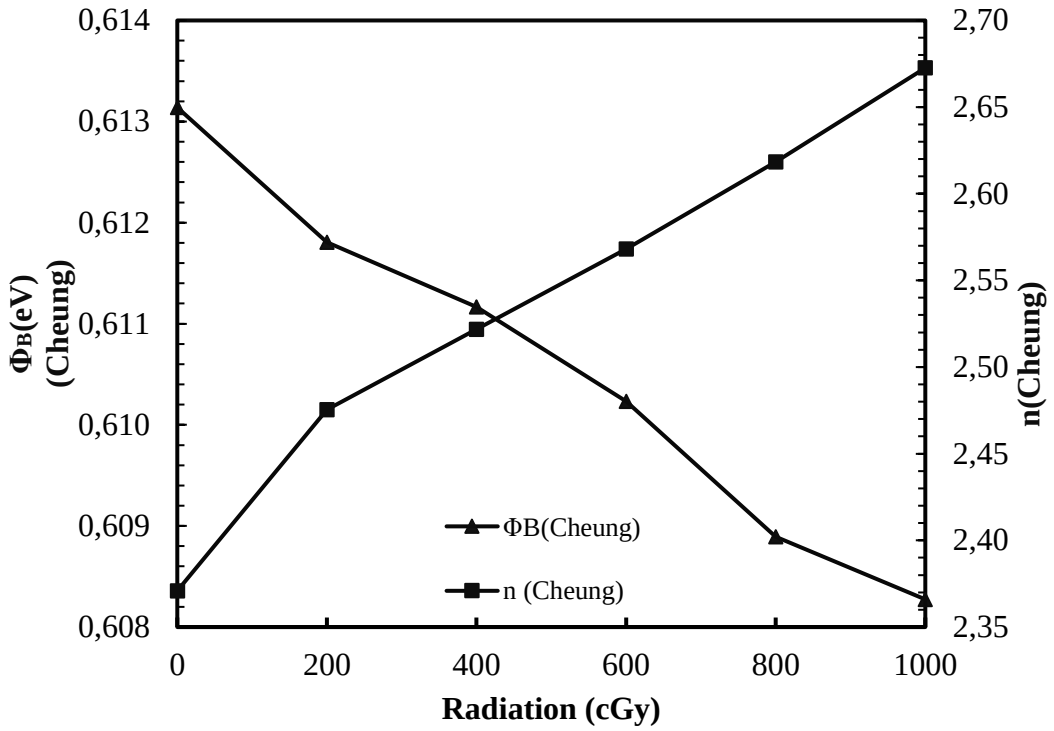


**Figure 6.7** The relation between the barrier height ($\Phi_B$(Cheung)) and the ideality factor (n(Cheung)) with irradiation.

**Table 6.3** The barrier height and the series resistance parameters calculated from electrical characteristics of the Mo/CuInGaTe$_2$/p-Si/Al structure as a function of testing radiation.

| | H(I)-I | | | | | |
|---|---|---|---|---|---|---|
| **Radiation (cGy)** | 0 | 200 | 400 | 600 | 800 | 1000 |
| **ΦB (eV)** | 0.613 | 0.612 | 0.611 | 0.610 | 0.609 | 0.608 |
| **Rs (kΩ)** | 1.885 | 2.472 | 2.706 | 2.882 | 3.056 | 3.268 |

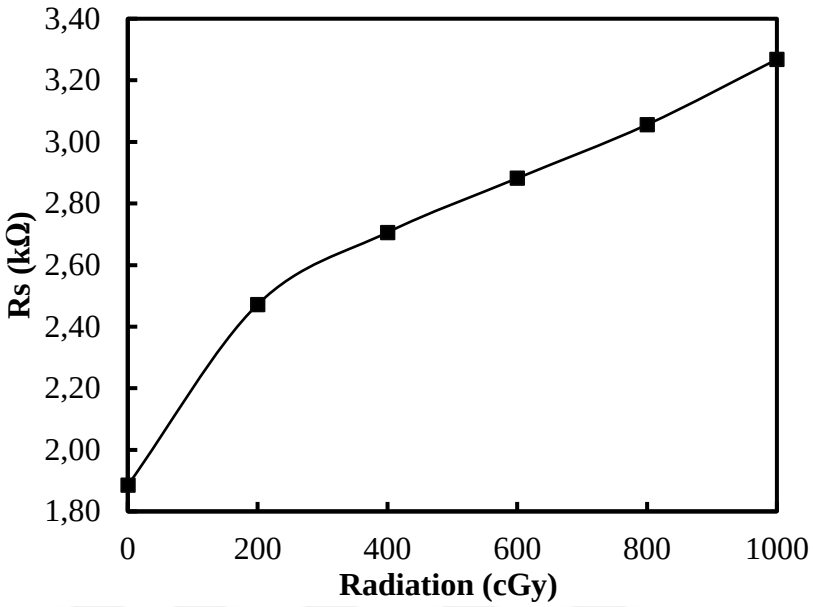


**Figure 6.8** The relation between the series resistance (Rs(H(I)-I)) and irradiation dose.

The resistance and ideality factors calculated from the I-V curve and Cheung's function show good agreement with each other [50].

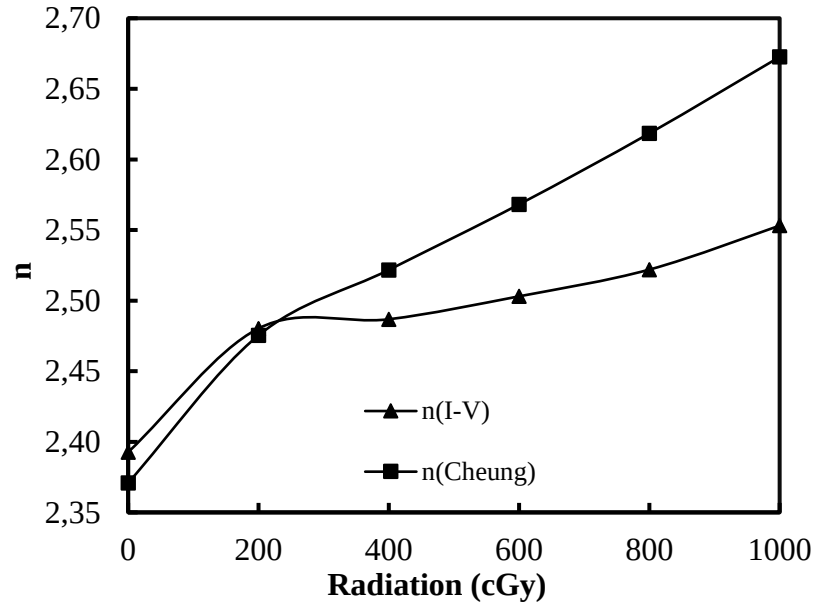


**Figure 6.9** Comparison of n(I-V) and n(Cheung) measurements with changing radiation.

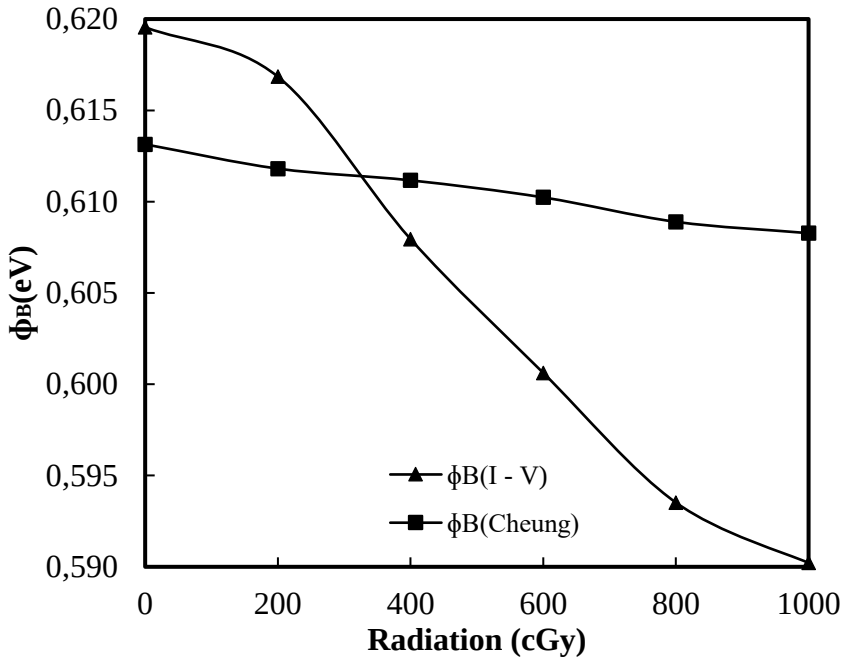


**Figure 6.10** Comparison of $\Phi_B$(I-V) and $\Phi_B$(Cheung) measurements with changing radiation.

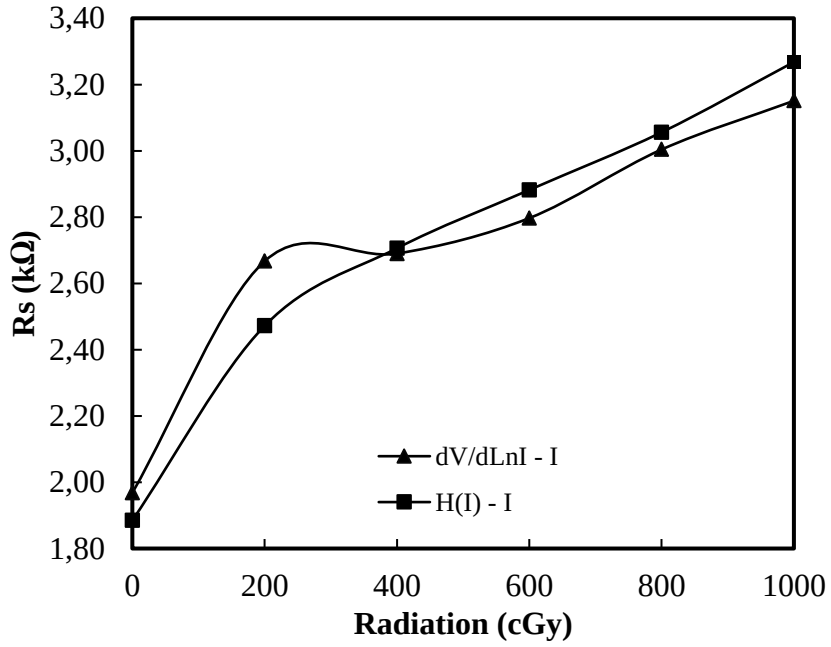


**Figure 6.11** Comparison of $R_S$(dV/dLnI-I) and $R_S$(H(I)-I) measurements with changing radiation.

The calculation of the energy-dependent distribution profiles of interface states are calculated using Equation **(6.14)** and Equation **(6.15)** from the forward bias I-V data for both before and after radiation and is given in Figure 6.12.

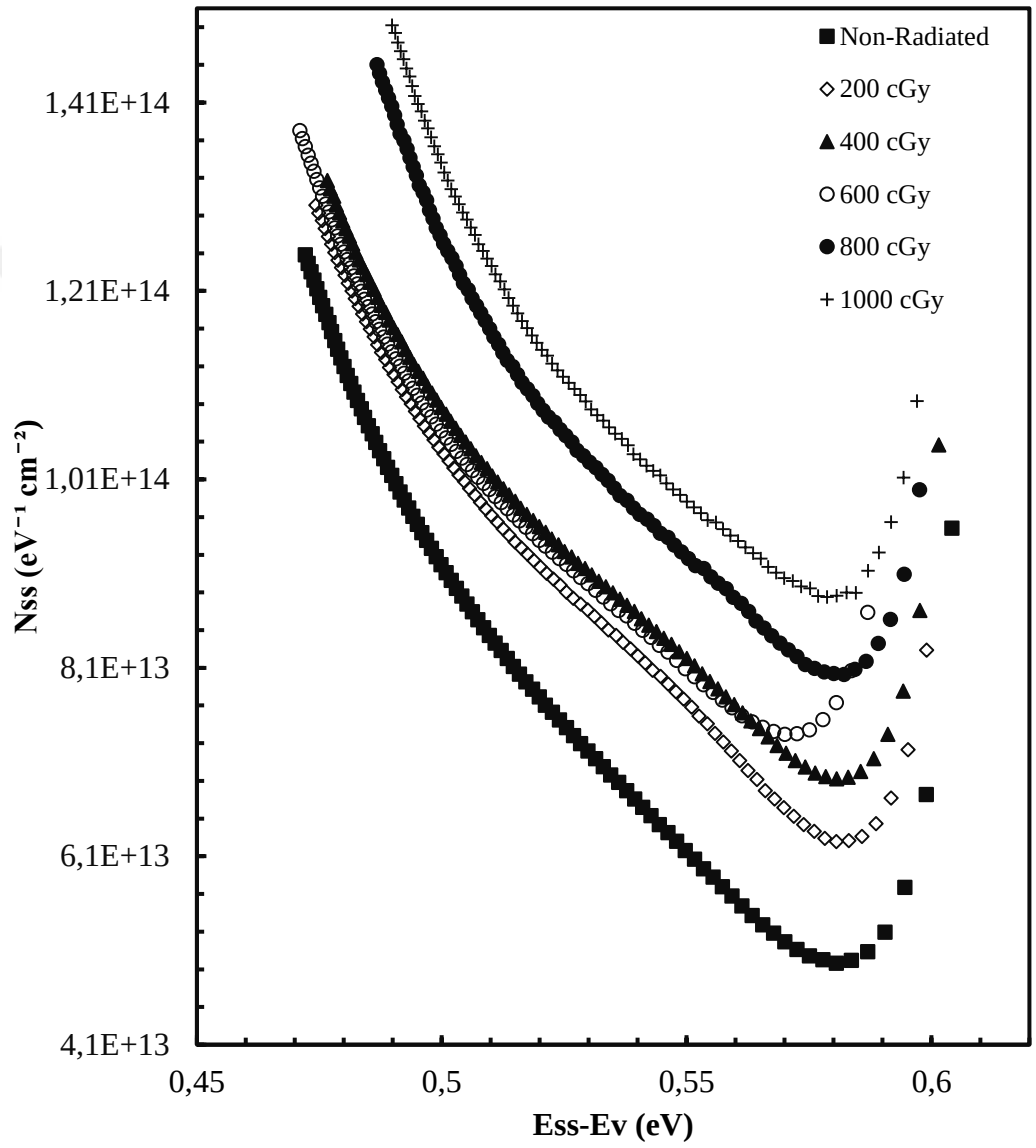


**Figure 6.12** The density of interface states vs. energy distribution profiles of the Mo/CuInGaTe$_2$/p-Si/Al diode.

Figure 6.13 shows SEM result of the $CuInGaTe_2$ thin film.

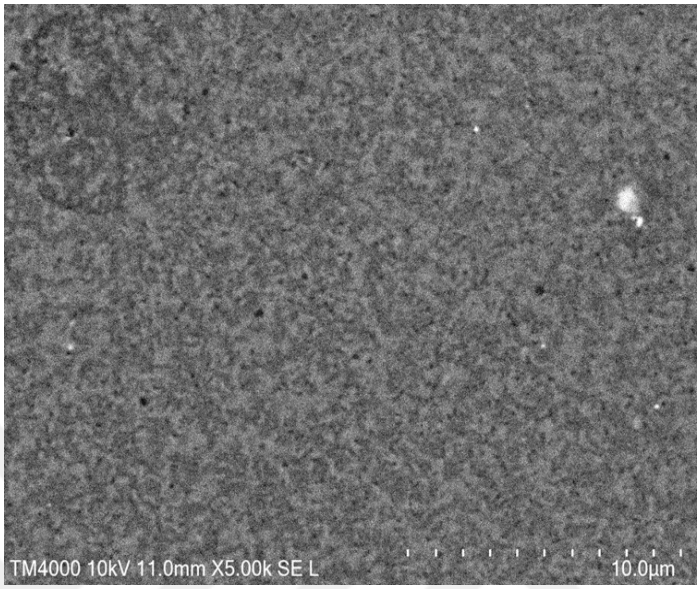


**Figure 6.13** Top view SEM result of the $CuInGaTe_2$ thin film.

Analyzing XRD pattern of the $CuInGaTe_2$ thin film in the 2Theta range$10^o$-$60^o$, with step size $2^o$, as seen Figure 6.14.

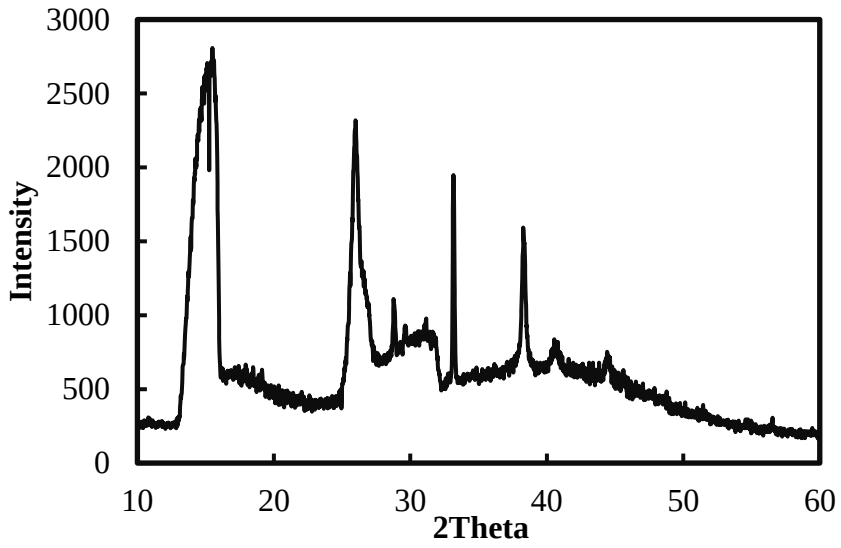


**Figure 6.14 X**-Ray diffraction data of the $CuInGaTe_2$ thin film.

## 6.4 Discussion and Conclusion

The forward bias current measurements as functions of applied voltage characteristics of the pre-radiated and irradiated samples were performed using a Keithley 2400 sourcemeter. The current was measured from 0 Volt to +1 Volt applied bias. Before and after irradiation, the I-V measurement of diodes were carried out at room temperature in darkness. 6 MV X-Ray beam, under 200, 400, 600, 800 and 1000 cGy radiation doses, was used to irradiate the samples in the direction normal to the sample.

In this work, the effect of ionizing X-Ray irradiation on a Mo/$CuInGaTe_2$/p-Si/Al diode is demonstrated by investigating its current-voltage characteristics. The diodes were exposed with 200,400, 600, 800 and 1000 cGy doses of irradiation. Various diode parameters were then determined by conventional I-V characterization and Cheung and Cheung's methods [51]. Additionally, the density of interface states vs. energy distribution profiles of the Mo/$CuInGaTe_2$/p-Si/Al diode was extracted from the forward bias I-V measurements. The junction obtained shows a non-ohmic and rectifying character [52].

Figure 6.4 and Figure 6.6 shows the experimental dV/dLnI vs. I and H(I) vs. I for the Mo/$CuInGaTe_2$/p-Si/Al diode at 300 K. H(I) vs. I mean while shows a straight line with the intercept at y-axis equal to $n\Phi_B$. $\Phi_B$ was obtained by substituting the n value from Equation **(6.7)** and the data of the downward curvature region in the forward bias I-V features from Equation **(6.9)**. The slope of this plot also limits $R_S$, which can be used to check the accuracy of Cheung and Cheung's method. From H(I) vs. I, the $\Phi$ and $R_S$ values were measured and presented in Tables 6.3. Equation **(6.7)** gives a straight line for the data of the downward curvature region in the forward bias I-V properties. Figure 6.4 shows the plot of dV/d(lnI) vs. I, from which the values of n and $R_S$ were calculated. As can be seen in the Table 6.4, the values of $R_S$ obtained from both dV/d(lnI) vs. I and H(I) vs. I plot are in near agreement with each other.

As shown in Table 6.4, from the forward bias current-voltage measurements, before irradiation and after 200,400,600,800 and 1000 cGy irradiation, ideality factors were

found to be 2.393, 2.480, 2.487, 2.503, 2.522 and 2.553, respectively and using the Cheung and Cheung's method were calculated 2.371, 2.475, 2.522, 2.568, 2.618 and 2.673 for the same radiation doses.

Ideality factor equals one for an ideal diode, which means that the resulting current is only due to thermionic emission. The tendency of the ideality factors to be greater than one for sample is an indication of deviation from the ideal according to the thermionic emission model [12, 53]. In this work, the n values demonstrated greater than unity values when operated in the voltage range between 0 and +1 V [54].

With increasing the testing radiation dose, the barrier height decreased from 0.620 eV at 200 cGy to 0.590 eV at 1000 cGy for I-V tests and from 0.613 eV to 0.608 eV from Cheungs' method. It is observed from the dV/dLnI-I plots, series resistances increased from 1.968 kΩ to 3.151 kΩ between the radiation doses of 200–1000 cGy and for the H(I)-I plot between 1.885 kΩ to 3.268 kΩ for the same radiation doses (Table 6.4).

**Table 6.4** Values of ideality factor, barrier height and series resistance.

| **Radiation (cGy)** | **n (I-V)** | **n Cheung** | **$\Phi_B$(eV) (I-V)** | **$\Phi_B$(eV) Cheung** | **$R_S$(kΩ) [dV/dLnI-I]** | **$R_S$(kΩ) [H(I)-I]** |
|---|---|---|---|---|---|---|
| **Non-Radiated** | 2.393 | 2.371 | 0.620 | 0.613 | 1.968 | 1.885 |
| **200** | 2.480 | 2.475 | 0.617 | 0.612 | 2.667 | 2.472 |
| **400** | 2.487 | 2.522 | 0.608 | 0.611 | 2.690 | 2.706 |
| **600** | 2.503 | 2.568 | 0.601 | 0.610 | 2.797 | 2.882 |
| **800** | 2.522 | 2.618 | 0.594 | 0.609 | 3.004 | 3.056 |
| **1000** | 2.553 | 2.673 | 0.590 | 0.608 | 3.151 | 3.268 |

As the applied voltage increased, the semi-logarithm I–V characteristics of the devices bend down (Figure 6.1), resulting in on-linear relationship between the logarithm of forward current and the applied voltage and indicating that the effect of series resistance became significant [55].

Rs caused the deviation from ideal thermionic emission theory. This deviation caused higher values n than unity while lowering barrier height values with increasing bias voltage and irradiation intensity [56].

Figure 6.3 and 6.7 show the ideality factor and barrier height as function of ionizing X-Ray radiation dose. A decrease in the values of barrier height and increase in the ideality factor are observed with increase in radiation dose. Irradiation might have introduced defects at the Mo/$CuInGaTe_2$/p-Si/Al interface leading to the reduction in semiconductor diode barrier height. Increase in the density of interface states can result in an increase in the ideality factor and lowering of the barrier height with dose [57]. An increase in the series resistance was found for all the doses indicating that product of mobility and free carrier concentration has reduced. The reduction in the mobility may be due to the introduction of defect centers on irradiation which act as scattering centers. Introduction of the deep traps result in decrease in carrier concentration will be reduced [58].

The interface state density vs. energy distribution curve of the Mo/$CuInGaTe_2$/p-Si/Al diode was obtained for the before and after radiations, using the forward bias I-V measurements, the voltage-dependent values of the ideality factor and potential barrier. As seen from Figure 6.12, the Nss values decrease with increasing energy from top of valence band toward mid-gap without any peak, and then increases. This confirms that the density of interface states changes with applied bias and each of applied biases corresponds to a position within the silicon gap [59]. As shown in Figure 6.12, the interface state density increases with the increase of the radiation value.

In this study, SEM was used to obtain high resolution topographical images of the samples. Surface image of the $CuInGaTe_2$ thin film is given in Figure 6.13. From the

Figure 6.13, $CuInGaTe_2$ thin film has been observed to have homogeneous and smooth surface.

In the XRD diffraction pattern, there are expansions, or furcations, at the base of the peaks (Figure 6.14). This shows us that there are defects in the crystal structure. The different intensity and peak widths seen in the XRD are an indication that the thin film is in the polycrystalline structure. Grain sizes directly give information about the quality of the crystal and are inversely proportional to the width of the diffraction peak obtained. That is, as the grain size gets smaller, the peak width increases.

To sum up briefly, these changes in the electrical properties of the Mo/$CuInGaTe_2$/p-Si/Al structures show that these diodes could be employed as sensing elements for the detection of ionizing X-Rays.

# REFERENCES

[1] Lukasiak, L., & Jakubowski, A., *"History of Semiconductors"*, Journal of Telecommunication and Information Technology, 1, 3-9, 2010.

[2] Morris, P.R., *"A History of the World Semiconductor Industry"*, Institution of Engineering and Technology, United Kingdom, 1990.

[3] Servagent, N., *"Fundamentals of Semiconductor physics* [online]*"*, France, http://www.optique-ingenieur.org/en/courses/OPI_ang_M05_C02/co/Contenu_10.html [Last Accessed: 11 July 2017].

[4] Belousov, A., *"Radiation Effects on Semiconductor Devices in High Energy Heavy Ion Accelerators"*, Thesis (Ph.D), Technische Universität Berlin, 2014.

[5] Glasstone, S., & Dolan, P.J., *"The Effects of Nuclear Weapons"*, (3th ed.), Prepared and Published by the United States Department of Defense and the Energy Research and Development Administration, United States of America, 1977.

[6] Kopp, C., *"The Electromagnetic Bomb - A Weapon of Electrical Mass Destruction"*, Report, Airpower Journal, March, 1-26, 1996.

[7] Trujillo Garcia, G., *"Control Dosimetrico Invivo en Radioterapia Externa u Sando Diodos Semiconductores"*, Revista Cubana de Oncologia, 14 (2), 129-135, 1998.

[8] Fiat Varol, S., & Polat, İ., & Bacaksız, E., & Kompitsas, M., & Çankaya, G., *"Electrical and Dielectrical Properties of Al/p-CIGSeTe/Mo Schottky Diodes"*, Current Applied Physics, 13 (6), 1112-1118, 2013.

[9] Fiat Varol, S., & Polat, İ., & Bacaksız, E., & Çankaya, G., & Koralli, P., & Manolakos, D.E., & Kompitsas, M., *"Optical and Structural Properties of Nanostructured* $CuIn_{0.7}Ga_{0.3}(Se_{(1-x)}Te_{(x)})_2$ *Chalcopyrite Thin Films-Effect of Stoichiometry and Annealing,"* Journal of Nanoscience and Nanotechnology, 14 (7), 1-9, 2014.

[10] Fiat, S., & Koralli, P., & Bacaksız, E., & Giannakopoulos, K.P., & Kompitsas, M., & Manolakos, D.E., & Çankaya, G., *"The Influence of Stoichiometry and Annealing Temperature on the Properties of* $CuIn_{0.7}Ga_{0.3}Se_2$ *and* $CuIn_{0.7}Ga_{0.3}Te_2$ *thin films"*, Elsevier, 545, 64-70, 2013.

[11] Fiat Varol, S., & Polat, İ., & Bacaksız, E., & Kompitsas, M., & Çankaya, G.,*"The Influence of Annealing Temperature and Tellurium (Te) on Electrical and Dielectrical Properties of Al/p-CIGSeTe/Mo Schottky Diodes"*, Current Applied Physics, 13(6), 1112-1118, 2013.

[12] Jaber Al-Ta'ii, H.M., & Periasamy, V., & Amin, Y.M., *"Electronic Properties of DNA-Based Schottky Barrier Diodes in Response to Alpha Particles"*, Sensors Open Access Journals, 15 (5), 11836-11853, 2015.

[13] Teffahi, A., & Hamri, D., & Abdelkader, M., & Saidane, A., & Alsaqri, N., & Felix, J.F., & Henini, M., *"Effect of* $^{60}Co$ *Gamma-Ray Irradiation on Electrical Properties of* $Ti/Au/GaAs_{1-X}N_x$ *Schottky Diodes"*, Current Applied Physics, 16 (8), 850-858, (2016).".

[14] Rao, A., & Krishnan, S., & Sanjeev, G., & Siddappa, K., *"Effect of 8 MeV Electrons on Au/n-Si Schottky Diodes"*, International Journal of Pure and Applied Physics, 5 (1), 55-62, 2009.".

[15] Taşçıoğlu, İ., &. Tataroğlu, A., & Özbay, A., & Altındal, Ş., *"The Role of 60Co γ-Ray Irradiation on the Interface States and Series Resistance in MIS Structures"*, Radiation Physics and Chemistry, 79 (4), 457-461, 2010.".

[16] Baran, H.M., & Tataroğlu, A., & Ertuğrul, R., *"Investigation of the Effects of Gamma-Ray Irradiation on Electrical Characteristics of MOS Capacitors"*, Optoelectronics and Advanced Materials Rapid Communications, 14 (3), 304-308, 2012.

[17] Mohd Husin Seria, D.F., & Mohamad, K.A., & Rusnan, F.N., & Ghosh, B.K., & Alias, A., & Saad, I., *"Flexible Spray Coated TIPS-Pentacene Organic PN Junction Diode"*, Journal of Advanced Research in Materials Science, 14 (1), 8-13, 2015.

[18] Neamen, D.S., *"Semiconductor Physics and Devices"*, (4th ed.), The McGraw Hill Companies, United States of America, 2012.

[19] SZE, S.M., & NG, K.K., *"Physics of Semiconductor Devices"*, (3rd ed.), John Wiley & Sons, New Jersey, 2007.

[20] Krishnan, S., *"AIEEE Physics"*, Sura College of Competition, Chennai, 2006.

[21] Salivahanan, S., & Suresh Kumar N., & Vallavaraj, A., *"Electronic Devices and Circuits"*, (2nd ed.), Tata McGraw Hill Publishing Company Limited, New Delhi, 2008.

[22] Coropceanu, V., & Cornil, J., & Silva Filho, D.A., & Olivier, Y., & Silbey, R., & Bredas, J. L., *"Charge Transport in Organic Semiconductors"*, Chemical Reviews, 107 (4), 926-952, 2007.

[23] Shaik, A., *"Physics and Radio-Electronics* [Online]*"*, Rajampet, http://www. physics-and-radio-electronics.com/electronic-devices-and-circuits/semiconduct or/electronand-hole-mobility.html [Last Accessed: 20 April 2017].

[24] Fonstad, C.G., *"Microelectronic Devices and Circuits"*, (Electronic ed.), McGraw-Hill, United States of America, 2006.

[25] Moll, J., *"The Evolution of the Theory for the Voltage-Current Characteristic of PN Junctions"*, Proceedings of the IRE, 46 (6), 1076-1082, 1958.

[26] Banyamin, Z.Y., *"Novel Photovoltaic Solar Power Generating Diode"*, Thesis (Ph.D), Manchester Metropolitan University, 2014.

[27] Razeghi, M., *"Fundamentals of Solid State Engineering"*, (3rd ed.) Springer Science & Business Media, New York, 2009.

[28] Van Zeghbroeck, B., *"Principles of Electronic Devices* [Online]*"*, Colorado, https://ece e.colorado.edu/~bart/book/book/chapter4/ch4_2.htm [Last Accessed: 16 May 2017]

[29] Papadopoulos, C., *"Solid-State Electronic Devices"*, (1st ed.), Springer-Verlag, New York, 2014.

[30] Rizzoni, G., *"Principles and Applications of Electrical Engineering"*, (5th ed.), McGraw-Hill Education, London, 2005.

[31] Weatherford, T.R., *"EC3220 Lecture Notes"*, Naval Postgraduate School, Monterey, California, 2002.

[32] Gladney, D.C., *"Simulating radiation-induced defects on semiconductor devices"*, Thesis (M.Sc.), Naval Postgraduate School, 2004.

[33] National Aeronautics and Space Administration (NASA), *"Solar Cell Array Design Handbook"*, vol. 1, Jet Propulsion Laboratory, California, 1976.

[34] Messenger, G.C., & Ash, M.S., *"The Effects of Radiation on Electronic Systems"*, (1st ed.), Van Nostrand Reinhold Company, New York, 1986.

[35] Spieler, H., *"Introduction to Radiation-Resistant Semiconductor Devices and Circuits"*, Ernest Orlando Lawrence Berkeley National Laboratory, Berkeley, USA, 1999.

[36] *"Radiation Tolerant and Radiation Hardened Microelectronics"*, [http://www.-mrcmicroe.com/Radiation_Effects.htm], [Last Accessed: 15 July 2003].

[37] Michalopoulos, P., *"Novel Approach for the Development and Optimization of State-of-the-Art Photovoltaic Devices Using Silvaco"*, Thesis (M.Sc), Naval Postgraduate School, 2002.

[38] Priyadarshi, S., & Dubey, V., & Dubey, S., *"Effect of Various Radiations on the Working of PN Junction Diode"*, International Journal of Advanced Research in Electrical, Electronics and Instrumentation Engineering, 6 (5), 4016-4023, 2017.

[39] Hardy, N., *"What is Thin Film Deposition By Thermal Evaporation?* [Online]*"*, United States of America, http://www.semicore.com/news/71-thin-film-depositi on-thermal-evaporation, [Last Accessed: 22 May 2017].

[40] Şahin, Y., *"The Effects of X-Ray Irradiation on the Current-Voltage (I-V) Characteristics of Metal/Organic/Semiconductor Rectifier Contacts"*, Thesis (M.Sc), Atatürk University, 2014.

[41] "*X-Işınları ve Kullanım Alanları*" [Online]. Available: https://neu.edu.tr/wp-content/uploads/2015/11/BMT-211-ders-notu-X-Isinlari.pdf, [Last Accessed: 1 April 2018].

[42] Fiat, S., *"The Production of $CuIn_{0.7}Ga_{0.3}(Se_{(1-x)}Te_x)_2$ Thin Films, Analyzing of the Structural, Morphological and Optical Properties"*, Thesis (M.Sc.), Gaziosmanpaşa University, 2012.

[43] Khakbaz, M., & Gholami, S., *"Measurement of I-V Characteristics of a PtSi/p-Si Schottky Barrier Diode at Low Temperatures"*, World Academy of Science, Engineering and Technology, 5 (9), 1285-1288, 2011.

[44] Cheung, S., & Cheung, N., *"Extraction of Schottky Diode Parameters from Forward Current-Voltage"*, Applied Physics Letters, 49 (2), 85-87, 1986.

[45] Cova, P., & Singh, A., & Medina, A., & Masut, R.A., *"Effect of Doping on the Forward Current-Transport Mechanisms in A Metal–Insulator Semiconductor Contact to InP:Zn Grown by Metal Organic Vapor Phase Epitaxy"*, Solid-State Electron. 42 (4), 477-485, 1998.

[46] Chand, S., & Kumar, J., *"Evidence for the Double Distribution of Barrier Heights in $Pd_2Si$/n-Si Schottky Diodes from I-V-T Measurements"*, Semiconductor Science Technology, 11 (8), 1203-1208, 1996.

[47] Card, H.C., & Rhoderick, E.H., *"Studies of tunnel MOS diodes I. Interface effects in silicon Schottky diodes"*, Journal of Physics D, Applied Physics, 4 (10), 1589-1601, 1971.

[48] Akkal,, B. & Benemara, Z., & Boudissa, A., & Bouiadjra, N.B., & Amrani, M., & Bideux, L., & Gruzza, B., *"Modelization and Characterization Of Au InSb/InP Schottky Systems as a Functıon of Temperature"*, Materials Science & Engineering. B, Solid-State Materials for Advanced Technology, 55 (3), 162-168, 1998.

[49] Singh, A., *"Characterization of Interface States at Ni/n$CdF_2$ Schottky Barrier Type Diodes and the Effect of $CdF_2$ Surface Preparation"*, Solid State Electronics, 28 (3), 223-232, 1985.

[50] Suhail, M.H., & Ibrahim, I.M., & Ahmad, Z., & Abdullah S.M., & Sulaiman, K., *"ITO/PEDOT: PSS/MEH:PPV/Alq3/LiF/Au as a Schottky Diode"*, International Journal of Application or Innovation in Engineering & Management (IJAIEM), 2 (1), 2013.

[51] Yang, Z., & Ma, Y., & Gong, M., & Li, Y., & Huang, M., & Gao, B., & Zhao, X., *"Recrystallization Effects of Swift Heavy $^{209}$Bi Ions Irradiation on Electrical Degradation in 4H-SiC Schottky Barrier Diode"*, Nuclear Instruments and Methods in Physics Research Section B: Beam Interaction with Materials and Atoms, 401, 51-55, 2017.

[52] Mohd Husin Seria, D.F., & Mohamad, K.A., & Rusnan, F.N., & Ghosh, B.K., & Alias, A.S.I., *"Flexible Spray Coated TIPS-Pentacene Organic PN Junction Diode"*, Journal of Advanced Research in Materials Science, 14 (1), 8-13, 2015.

[53] Fiat Varol, S., & Bacaksız, E., & Kompitsas, M., & Çankaya, G.,"Temperature and Tellurium (Te) Dependence of Electrical Characterization and Surface Properties for a Chalcopyrite Structured Schottky Barrier Diode", 585, 178-184,2014.

[54] Güllü, Ö., & Çankaya, M., & Barış, Ö., & Türüt, A., *"DNA-Based Organic-on-Inorganic Devices: Barrier Enhancement and Temperature Issues"*, Microelectronic Engineering, 85 (11), 2250-2255, 2008.

[55] Lioliou, G., & Meng, X., & Ng, J.S., & Barnett, A.M.,"*Characterization of Gallium Arsenide X-Ray Mesa p-i-n"*, 813, 1-9, 2015.

[56] Çulcu, H., & Gökçen, M., & Allı, A., & Allı, S., *"Current-Voltage Characteristics of Au/PLiMMA/n-Si Diode Under Ultraviolet Irradiation"*, Journal of Physics and Chemistry of Solids, 103, 197-200, 2017.

[57] Nigam, S., & Abernathy, C.R., & Allums, K.K., & Chung, G.Y., & Dwivedi, R., & Fogarty Kim, J., & Mac Millan, M.F., & Pearton, S., & Ren, F., & Williams, J.R., & Wilkins, T.N., "High Energy Proton Irradiation Effects on SiC Schottky Rectifiers", Applied Physics Letters, 81 (13), 2385-2387, 2002.

[58] Chand, S., & Kumar, J., *"Current-Voltage Characteristics and Barrier Parameters of $Pd_2Si$/p-Si (111) Schottky Diodes in a Wide Temperature Range"*, Semiconductor Science and Technology, 10 (12) , 1680-1688, 1995.

[59] Sönmezoğlu, S., & Şenkul, S., & Taş, R., & Çankaya, G., & Can, M., *"Electrical and Interface State Density Properties of Polyaniline–Poly-3-Methyl Thiophene Blend/p-Si Schottky Barrier Diode"*, Solid-State Sciences,12 (5), 706-711, 2010.